Received: 17 January 2018 | Revised: 16 July 2018 | Accepted: 15 August 2018

DOI: 10.1002/nme.5950

RESEARCH ARTICLE

WILEY

A quasi-incompressible and quasi-inextensible element formulation for transversely isotropic materials

H. Dal

Department of Mechanical Engineering, Middle East Technical University, Ankara, Turkey

Correspondence
H. Dal, Department of Mechanical Engineering, Middle East Technical University, Dumlupinar Bulvari 1, 06800 Ankara, Turkey.
Email: dal@metu.edu.tr

Funding information
Tübitak Bideb 2232, Grant/Award Number: 114C073

Summary

The contribution presents a *new* finite element formulation for quasi-inextensible and quasi-incompressible finite hyperelastic behavior of transversely isotropic materials and addresses its computational aspects. The material formulation is presented in purely *Eulerian* setting and based on the additive decomposition of the free energy function into isotropic and anisotropic parts, where the former is further decomposed into isochoric and volumetric parts. For the quasi-incompressible response, the *Q1P0* element formulation is outlined briefly, where the pressure-type Lagrange multiplier and its conjugate enter the variational formulation as an extended set of variables. Using the similar argumentation, an extended Hu-Washizu–type mixed variational potential is introduced, where the volume averaged fiber stretch and fiber stress are additional field variables. Within this context, the resulting Euler-Lagrange equations and the element formulation resulting from the extended variational principle are derived. The numerical implementation exploits the underlying variational structure, leading to a canonical symmetric structure. The efficiency of the proposed approached is demonstrated through representative boundary value problems. The superiority of the proposed element formulation over the standard *Q1* and *Q1P0 element formulation* is studied through convergence analyses. The proposed finite element formulation is modular and exhibits very robust performance for fiber reinforced elastomers in the inextensibility limit.

KEYWORDS

anisotropy, hyperelasticity, mixed finite element design, mixed variational principles, quasi-incompressiblity, quasi-inextensibility

1 | INTRODUCTION

Anisotropic materials either naturally exist, eg, biological tissues and wood, or manufactured, eg, composite materials and fiber reinforced elastomers. The glass, aramid, or steel cord reinforcement embedded into rubberlike materials increases the directional stiffness considerably. Both elastomers and biological tissues exhibit nearly incompressible mechanical response. Therefore, development of efficient and robust finite element formulations in the quasi-incompressible and quasi-inextensible limit is of great interest for the analysis of such materials.

Rubberlike materials and soft biological tissues exhibit very stiff volumetric response compared to bulk shear response. This nearly incompressible mechanical response causes the well-known *locking phenomena*. Herein, the standard

bilinear or trilinear shape functions can incorporate the incompressiblity constraint at the expense of artificial stiffening.[1,2] The finite element method based on standard displacement formulations exhibits very poor performance in the quasi-incompressible limit, where the bulk modulus is two to three orders of maginute higher than the shear modulus. This effect is more pronounced in thin structural members under bending dominated loading. Since the stiffness of fiber reinforced polymers along fiber directions is considerably higher compared to that in transverse direction, a similar mathematical problem arises in the inextensibility limit for the fiber reinforced polymers and biological tissues.[3,4]

One solution to the problem is to use *h*- or *p*-refinement strategies. Locking response is known to vanish for high-order triangles $p > 4$.[5] Use of lower-order elements with *h*-refinement increases the computational cost. Nonetheless, low-order elements remain popular due to their simplicity and robustness compared to higher-order elements especially in case of nonlinear Lagrangian hyperelastic formulations.[6] Within this context, improving the performance of standard lower-order elements has become an area of intense research in the last three decades. The locking problem can be circumvented by various methodologies such as *reduced integration*, *stabilization*, and *mixed or hybrid element formulations*.[7]

Mixed or *hybrid element formulations* are based on variational methods, where an additional stress or strain-type penalty term is introduced as a Lagrange multiplier. In linear elasticity, the first hybrid formulation was proposed by Pian et al[8-10] based on Hellinger-Reissner variational principle for linear elastic solids. These elements improve stress approximation of the standard displacement formulations under extreme distortions. They require matrix inversion of the elasticity tensor at element level that is not straightforward in case of nonlinear elasticity at finite strains.[11] One strategy to improve the behavior of linear finite elements for pure displacement formulations against locking phenomenon is to use *reduced integration schemes* along with *stabilization techniques*.[1,12] Use of less Gauss points than required for the assembly of the tangent and residual terms for the polynomial shape functions can be traced back to the work of Zienkiewicz et al.[13] The reduced integration results in the *hourglass modes* or *zero energy modes*, which need to be stabilized.[14,15] The nonphysical eigenforms appear as hourglass forms, which brought up the term hourglass instability. Reduced integration along with hourglass stabilization methods is computationally feasible as they reduce the number of computations at element level. On the other hand, such stabilization schemes usually come with the expense of introduction of additional nonphysical parameters into the formulation, which might affect the results under bending dominated problems. In this context, *enhanced strain formulations* (ESFs) were developed[6,16-20] for finite strain elasticity and elastoplasticity problems. These formulations are based on the introduction of auxiliary incompatible strain field, which satisfy the material frame invariance and objectivity requirements. They are based on Hu-Washizu–type variational principles.[21,22] Extension of such formulations to the higher-order gradient plasticity has been treated in the works of Miehe et al.[23-25] Incorporation of the ESFs does not require the modification of the constitutive model. However, nonlinear ESFs exhibit nonphysical instabilities on element level, which cannot be eliminated by increasing the order of quadrature or by exchanging the material model. The element formulation can be elaborated to alleviate these hour-glass–type instabilities by introducing canceling terms at element level.[26,27] These element formulations are successful in elimination of the hourglass modes under compression but numerical stability cannot be ensured for irregular distorted meshes and nonhomogeneous stress states. The separation of the element tangent matrix into constant and hourglass parts, and by introducing a control technique based on a modal analysis, the hourglass instabilities can be overcome even for highly distorted meshes (see the works of Reese and Wriggers[28,29]).

The *mean dilatation approach* or the so-called *Q1P0*, element formulation was introduced by Nagtegaal et al[30] and contained in the monogragh of Brezzi and Fortin[31] for small-strain problems and was extended to large-strains by Simó et al.[32] It has been applied to principal invariant-based hyperelastic materials in the quasi-incompressible limit by Simó and Taylor.[33] The element formulation is based on the introduction of an additional term into the potential functional, which acts as a constraint imposing the incompressibility via a penalty parameter. The model is well documented in the works of Wriggers[7] and Miehe.[34] The *Q1P0* formulation is recovered in the assumed ESF, where the latter approach performs relatively better in bending dominated problems. However, the former approach has gained a wide acceptance in the mechanics of rubberlike materials, whereas the latter is adopted in the finite element implementation of elasto-plastic material response.[35] The use of *Q1P0* element in the context of transversely anisotropic materials and soft tissues have been demonstrated in the work of Weiss et al.[36]

The stability of the mixed finite element methods is validated through the *LBB condition*, also known as the *inf-sup condition*.[37-39] The stability of incompressible materials for linear elasticity was treated in the work of Bathe.[40] However, the investigation of the inf-sup condition is not trivial at finite strain setting. The *Q1P0* fails to satisfy the LBB condition in the geometrically linear setting.[7] However, it has been proven to be stable for a wide range of applications of quasi-incompressible materials undergoing large deformations.[34]

The free energy function of isotropic solids can be modeled through three irreducible invariants $\{I_1, I_2, I_3\}$, which constitute the integrity basis of the deformation tensor.[41] For incompressible materials, the two irreducible invariants $\{I_1, I_2\}$ are enough to describe the incompressible isotropic deformation. For transversely anisotropic solids, one can introduce additional set of irreducible invariants $\{I_4, I_5\}$ with the help of the structural tensors that satisfy the objectivity requirement under superimposed rigid body rotations.[42-44] In unidirectional fiber reinforced materials, the stored energy can be obtained in terms of a free energy for the unreinforced base matrix with arguments augmented by the fourth invariant I_4 related to the fiber stretch as an additional penalty function for stretching in the fiber direction.[45] A similar approach can be adopted for the modeling of soft biological tissues.[46] The latter function is also known as the *standard reinforcing model* (see the work of Qiu and Pence[45]). Therein, loss of monotonicity under simple shear and uniaxial compression were detected as the fiber stiffness increases. The material instabilities in terms of loss of ellipticity of the standard reinforcing model were treated in other works.[47-49] The behavior of transversely isotropic solid with inextensible unidirectional reinforcement is studied in the work of Adkins and Rivlin.[50]

It has been a common practice to split the free energy into purely volumetric part as a function of $J = \det \boldsymbol{F}$ and an isochoric part, which is a function of the unimodular part of the deformation gradient $\bar{\boldsymbol{F}} = J^{-1/3}\boldsymbol{F}$ (see the work of Flory[51]). This split has superior advantages in the incompressibility limit, giving rise to the easy implementation of the *mean dilatation approach* into the finite element formulation. On the other side, it might lead to unphysical results in the compressible region.[52] A similar anomaly has been detected for the split of the free energy into isotropic and anisotropic parts as well. It has been shown that the volumetric-isochoric split should be applied to the matrix part only.[53] The nonphysical effect arising due to use of the fourth invariant $\bar{I}_4$ of the unimodular stretch tensors is demonstrated in the work of Helfenstein et al[54] under unixial tension test in the fiber direction. Therein, uniaxial stress configurations reveal volume growth at rather small stretches, rendering a negative instantaneous Poisson ratio ν. This is due to the competition between exponential anisotropic free energy in the quasi-inextensibility limit and the (penalty) volumetric free energy throughout the minimization of the overall energy under unixaial tension. This competition can be remedied by taking the anisotropic free energy function $\psi_{\text{ani}} = \psi_{\text{ani}}(I_4)$ in terms of the fourth invariant of the deformation tensor.

Recently, Hu-Washizu–type mixed variational principles for the treatment of the inextensibility limit in fiber-reinforced materials and biological tissues have been studied in related works.[3,4,55,56] The element formulation of Zdunek et al[3,4] is based on the kinematic split of the deformation gradient into purely unimodular extensional part, a purely spherical part, and an extension free unimodular tensor. The Lagrangian element formulation is similar to the mean dilatational approach[32] (MDA) as it uses scalar conjugate pairs (p, θ) and (ρ, λ) for pressure-dilatation and fiber stress-stretch, respectively. This ansatz leads to a five-field variational formulation, where the consistent linearization and static condensation at element level lead to the purely displacement element matrix. In this formulation, the convergence and stability of the iterative solution scheme as well as the exact element assembly have not been presented. The formulation of Schröder et al[55] and the follow-up work of Wriggers et al[56] are however a hybrid model that combines the MDA for quasi-incompressibility and the ESF for the inextensibility with the help of a fiber stretch-type additional deformation measure into the variational formulation. Therein, the simplified kinematic approach for the anisotropy is adopted where the free energy is based on the additive decomposition into isotropic and anisotropic parts. The formulation is in Lagrangian setting and additional stiffness matrix terms due to the extra terms are eliminated through static condensation at element level.

The scope of this work is to introduce a theoretical and computational setting for nearly incompressible and inextensible material behavior based on a saddle point principle derived from a mixed potential. Within this context, a five-field Hu-Washizu–type extended variational formulation is proposed. It is shown that the variational derivatives of the mixed potential lead to the field equations governing the boundary value problem at hand. The result of the variational principle is a mixed finite element formulation, extending classical *Q1P0* element formulation or, in other words, the MDA,[32] to the inextensibility limit. To this end, the free energy function is additively decomposed into purely volumetric, purely isochoric parts for the isotropic response, and an additional part due the fiber reinforcement for the anisotropic part. On the kinematics side, the deformation gradient is multiplicatively decomposed into unimodular and spherical parts and the anistropy is modeled through the simplified kinematics approach with the help of the additional fourth invariant. Hence, the simple kinematics enables a straightforward extension of standard hyperelastic models to the quasi-inextensible setting due to unidirectional fiber reinforcement. Herein, the quasi-inextensiblity is enforced through and additional fiber stretch-type scalar kinematic variable λ and a Lagrange multiplier s, which can be interpreted as the mean fiber stress. The presented constitutive formulation is in the Eulerian setting based on the Kirchhoff stresses $\boldsymbol{\tau}$ and the Eulerian metric tensor $\boldsymbol{g}$. However, the finite element method is Lagrangian. The term *Eulerian* here refers to the stress and deformation measures used throughout the variational formulation. The interested reader is referred to the work of Demarco and

Dvorkin[57] for the Eulerian finite element method and the work of Carbonell and Carbonell[58] for the updated Lagrangian finite element method (see also the references therein). The resulting finite element formulation is very attractive because it is based on the direct homogenization of the additional field variables at element level through integration over the element domain in a preprocessing step. It can be combined with linear and higher-order element formulations in a straightforward manner because the implementation does not require any additional manipulation due to kinematics of the existing isotropic hyperelastic models. As a special case, the assembly of the element matrix for eight-noded brick element is demonstrated.

The paper is organized as follows. In Section 2, the multifield variational formulation, which leads to the quasi-incompressible and quasi-inextensible element formulation, will be introduced. The weak and strong forms in terms of Euler-Lagrange equations will be derived. Section 3 presents discrete counterpart of the weak forms obtained from the variation of the mixed potential. An eight-noded brick element for the *large strain* finite element analysis of quasi-incompressible and quasi-inextensible materials will be demonstrated as a special case in Section 4. In Section 5, the performance of the proposed element formulation is evaluated in terms of representative boundary value problems. The convergence and stability issues are investigated as well. The results are summarized in Section 6.

2 | GOVERNING EQUATIONS OF MOTION

This section introduces the field equations and corresponding state variables of a transversely isotropic hyperelastic solid body. The kinematics and integrity basis of the deformation and the constitutive equations based on Yeoh-type hyperelastic model are briefly introduced. The extension of the model to transverse anisotropy through standard reinforcing model is presented. Finally, the variational problem leading to the static equilibrium in the quasi-static limit is demonstrated.

2.1 | Geometric mappings and the field variables

A *body* $\mathscr{B}$ is a three-dimensional manifold consisting of material points $\mathscr{P} \in \mathscr{B}$. The motion of the body is defined by a one-parameter function of time via bijective mappings

$$\chi(\mathscr{P}, t) = \begin{cases} \mathscr{B} \to \mathscr{B}(\mathscr{P}, t) \in \mathbb{R}^3 \times \mathbb{R}_+ \\ \mathscr{P} \mapsto \boldsymbol{x} = \chi_t(\mathscr{P}) = \chi(\mathscr{P}, t). \end{cases} \tag{1}$$

The point $x = \chi(\mathscr{P}, t)$ denotes the configuration of the particle $\mathscr{P}$ at time $t \in \mathbb{R}_+$. Let the configuration of the material points at a reference time t_0 be denoted by $\boldsymbol{X} = \chi(\mathscr{P}, t_0) \in \mathbb{R}^3$ and $\chi_t(\mathscr{P}) = \chi(\mathscr{P}, t)$ denote the configuration for a frozen time frame t. Then, the placement map $\boldsymbol{\varphi}_t = \chi_t \circ \chi_{t_0}^{-1}(\boldsymbol{X})$ such that

$$\boldsymbol{\varphi}_t(\boldsymbol{X}) = \begin{cases} \mathscr{B}_0 \to \mathscr{B} \in \mathbb{R}^3 \\ \boldsymbol{X} \mapsto \boldsymbol{x} = \boldsymbol{\varphi}(\boldsymbol{X}, t) \end{cases} \tag{2}$$

maps the reference configuration $\boldsymbol{X} \in \mathscr{B}_0$ of a material point onto the spatial counterpart $\boldsymbol{x} \in \mathscr{B}$ (see Figure 1). The *deformation gradient*

$$\boldsymbol{F} : T_X\mathscr{B}_0 \to T_x\mathscr{B}; \quad \boldsymbol{F} := \nabla_X \boldsymbol{\varphi}_t(\boldsymbol{X}) \tag{3}$$

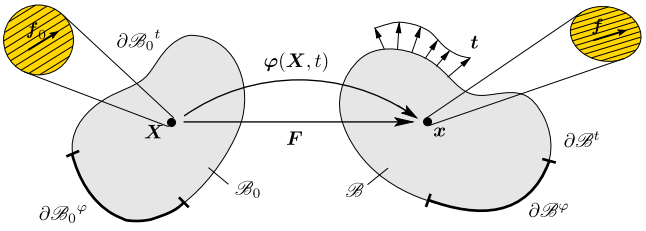

FIGURE 1 Nonlinear deformation of a solid. The reference configuration $\mathscr{B} \in \mathbb{R}^3$ and the spatial configuration $\mathscr{S} \in \mathbb{R}^3$. $\boldsymbol{\varphi} : \mathscr{B} \times \mathbb{R} \mapsto \mathbb{R}^3$ is the nonlinear placement field, which maps at time $t \in \mathbb{R}_+$ material point position $\boldsymbol{X} \in \mathscr{B}$ onto spatial position $\boldsymbol{x} = \boldsymbol{\varphi}(\boldsymbol{X}, t) \in \mathscr{S}$. The deformation gradient $\boldsymbol{F}$ maps a Lagrangian line element $\mathrm{d}\boldsymbol{X}$ onto its Eulerian counterpart $\mathrm{d}\boldsymbol{x} = \boldsymbol{F}\mathrm{d}\boldsymbol{X}$ [Colour figure can be viewed at wileyonlinelibrary.com]

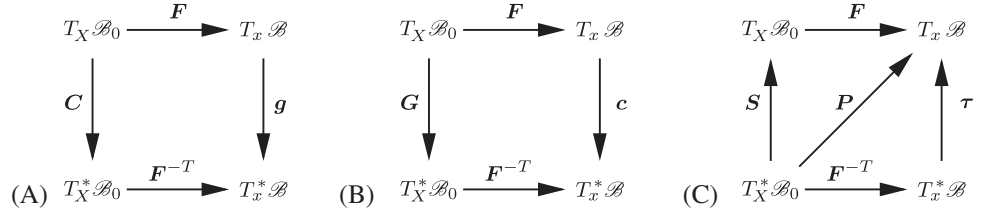

FIGURE 2 Definition of metric and stress tensors. A, *Current metric* in Lagrangian configuration $\boldsymbol{C} = \boldsymbol{F}^T\boldsymbol{g}\boldsymbol{F}$; B, *Reference metric* in Eulerian configuration $\boldsymbol{c} = \boldsymbol{F}^{-T}\boldsymbol{G}\boldsymbol{F}^{-1}$; C, relationship between stresses $\boldsymbol{\tau} = \boldsymbol{F}\boldsymbol{S}\boldsymbol{F}^T$. The Kirchhoff stress in the Eulerian configuration is *dual* to $\boldsymbol{g}$ and $\boldsymbol{c}$. The second Piola stress in the Lagrangian configuration is *dual* to $\boldsymbol{C}$ and $\boldsymbol{G}$

maps the unit tangent of the reference or the *Lagrangian* configuration onto its counterpart in the current or the *Eulerian* configuration. The gradient operators $\nabla_X[\bullet]$ and $\nabla_x[\bullet]$ denote the spatial derivative with respect to the reference $\boldsymbol{X}$ and current $\boldsymbol{x}$ coordinates, respectively. Let $d\boldsymbol{X}$, $d\boldsymbol{A}$, and dV denote the infinitesimal line, area, and volume elements in the undeformed configuration. Then, the deformation gradient $\boldsymbol{F}$, its cofactor $\text{cof}[\boldsymbol{F}] = \det[\boldsymbol{F}]\boldsymbol{F}^{-T}$, and the Jacobian $J := \det[\boldsymbol{F}] > 0$ characterize the deformation of infinitesimal line, area, and volume elements

$$d\boldsymbol{x} = \boldsymbol{F}d\boldsymbol{X}, \qquad d\boldsymbol{a} = \text{cof}[\boldsymbol{F}]d\boldsymbol{A}, \qquad dv = JdV. \tag{4}$$

The condition $J := \det[\boldsymbol{F}] > 0$ ensures the nonpenetrable deformations $\boldsymbol{\varphi}$. Furthermore, reference $\mathscr{B}_0$ and the spatial $\mathscr{B}$ manifolds are locally furnished with the covariant reference $\boldsymbol{G}$ and current $\boldsymbol{g}$ metric tensors in the neighborhoods $\mathcal{N}_X$ of $\boldsymbol{X}$ and $\mathcal{N}_x$ of $\boldsymbol{x}$, respectively. These metric tensors are required for the mapping between the co and contravariant objects in the Lagrangian and Eulerian manifolds.[59] To this end, the *right Cauchy Green tensor* and the inverse of the *left Cauchy Green tensors* are defined

$$\boldsymbol{C} = \boldsymbol{F}^T\boldsymbol{g}\boldsymbol{F} \quad \text{and} \quad \boldsymbol{c} = \boldsymbol{F}^{-T}\boldsymbol{G}\boldsymbol{F}^{-1} \tag{5}$$

as the pull back of the current metric $\boldsymbol{g}$ and push forward of the Lagrangian metric $\boldsymbol{G}$, respectively. The *left Cauchy Green tensor* or the *Finger tensor* is denoted by $\boldsymbol{b} = \boldsymbol{c}^{-1}$. For a geometric interpretation, we refer to Figures 2A-B. In order to impose the quasi-incompressible nature of the rubberlike materials and soft biological tissues, the deformation gradient $\boldsymbol{F}$ is decomposed into volumetric $\boldsymbol{F}_{\text{vol}} := J^{1/3}\boldsymbol{1}$ and unimodular $\bar{\boldsymbol{F}} := J^{-1/3}\boldsymbol{F}$ parts

$$\boldsymbol{F} = \boldsymbol{F}_{\text{vol}}\bar{\boldsymbol{F}}. \tag{6}$$

In order to extend the isotropic continuum, we introduce the Lagrangian unit vector $\boldsymbol{f}_0$ such that

$$|\boldsymbol{f}_0|_G = 1, \quad \text{where} \quad |\boldsymbol{f}_0|_G = \left(\boldsymbol{f}_0 \cdot \boldsymbol{G}\boldsymbol{f}_0\right)^{1/2}. \tag{7}$$

Under the action of $\boldsymbol{\varphi}_t$, the Eulerian counterpart is obtained through the tangent map as

$$\boldsymbol{f} = \boldsymbol{F}\boldsymbol{f}_0. \tag{8}$$

The boundary of the solid domain can be decomposed into Dirichlet and Neumann-type boundaries, such that $\partial\mathscr{B} = \partial\mathscr{B}^\varphi \cup \partial\mathscr{B}^t$ and $\partial\mathscr{B}^\varphi \cap \partial\mathscr{B}^t = \emptyset$.

2.1.1 | Stress tensors

Consider a part $\mathscr{P}_0 \subset \mathscr{B}_0$ cut out of the reference configuration $\mathscr{B}_0$ and its spatial counterpart $\mathscr{P}_t \subset \mathscr{B}_t$, with boundaries $\partial\mathscr{P}_0$ and $\partial\mathscr{P}_t$, respectively. The total stress vector $\boldsymbol{t}$ acts on the surface element $d\boldsymbol{a} \subset \partial\mathscr{P}_t$ on the deformed configuration and represents the force that the rest of the body $\mathscr{B}_t \backslash \mathscr{P}_t$ exerts on $\mathscr{P}_t$ through $\partial\mathscr{P}_t$. Cauchy's stress theorem establishes a linear dependence between the traction and the outward surface normal

$$\boldsymbol{t}(\boldsymbol{x}, t; \boldsymbol{n}) = \boldsymbol{\sigma} \cdot \boldsymbol{n} \tag{9}$$

through the total Cauchy stress tensor $\boldsymbol{\sigma}$. We define the Lagrangian and Eulerian unit area elements

$$d\boldsymbol{A} = \boldsymbol{N}dA \quad \text{and} \quad d\boldsymbol{a} = \boldsymbol{n}da, \tag{10}$$

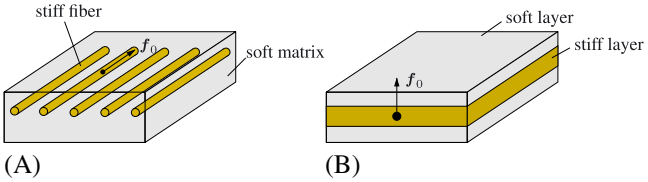

FIGURE 3 Transverse anisotropy. A, stiff fibers embedded in soft matrix; B, composite laminate consisting of stiff and soft layers [Colour figure can be viewed at wileyonlinelibrary.com]

where $\boldsymbol{N}$ and $\boldsymbol{n}$ are the surface normals of the undeformed and defored solid body. Now, consider the identity $\boldsymbol{T}d\boldsymbol{A} = \boldsymbol{t}d\boldsymbol{a}$ by scaling the (true) spatial force $\boldsymbol{t}d\boldsymbol{a}$ by the reference area element $d\boldsymbol{A}$. This induces the definition of the nominal or the *first Piola-Kirchhoff* stress tensor $\boldsymbol{P}$ by setting

$$\boldsymbol{P}d\boldsymbol{A} = \boldsymbol{\sigma}d\boldsymbol{a}, \quad \text{where} \quad \boldsymbol{P} := J\boldsymbol{\sigma}\boldsymbol{F}^{-T}. \tag{11}$$

2.2 | Constitutive model: transversely isotropic Yeoh model

2.2.1 | The free energy function

Fiber reinforced elastomers, eg, *carbon* and *aramid* reinforced elastomers, exhibit nearly incompressible bulk response and nearly inextensible response in the reinforcement direction (see Figure 3B). For elastomers with one fiber family, we postulate the specific form of the Helmholtz free energy function

$$\psi(\boldsymbol{g};\boldsymbol{F},\boldsymbol{f}_0) := \psi_{\text{vol}}(J) + \psi_{\text{iso}}(\boldsymbol{g};\bar{\boldsymbol{F}}) + \psi_{\text{ani}}(\boldsymbol{g};\boldsymbol{F},\boldsymbol{f}_0), \tag{12}$$

which additively decomposed into volumetric, isochoric, and anisotropic parts, respectively. It is defined with respect to unit reference volume. We construct *Q1P0F0* mixed-element formulation for fiber-reinforced rubbery polymers in terms of a quasi-incompressible Yeoh-type hyperelelastic formulation in the decoupled form (12). However, the formulation is general and can be used in combination of any isotropic hyperelastic solid model. The free energy stored in an isotropic hyperelastic material is governed by three invariants, ie,

$$I_1 := \text{tr}\,\boldsymbol{C}, \quad I_2 := \frac{1}{2}\left[I_1^2 - \text{tr}(\boldsymbol{C}^2)\right], \quad \text{and} \quad I_3 := \det\boldsymbol{C} = J^2, \tag{13}$$

of the right Cauchy Green tensor $\boldsymbol{C} = \boldsymbol{F}^T\boldsymbol{g}\boldsymbol{F}$. Moreover, the anisotropic response of hyperelastic materials requires the description of additional invariants. To this end, the two additional invariants are defined in terms of reference unit vector $\boldsymbol{f}_0$

$$I_4 := \boldsymbol{f}_0 \cdot \boldsymbol{C}\boldsymbol{f}_0 \qquad I_5 = \boldsymbol{f}_0 \cdot \boldsymbol{C}^2\boldsymbol{f}_0, \tag{14}$$

which idealize the energy storage due to a single fiber reinforced microstructure for rubberlike materials. The volumetric part of the free energy function (12), ie,

$$\psi_{\text{vol}}(J) = \frac{\kappa}{4}\left(J^2 - 2\ln J - 1\right), \tag{15}$$

enforces the quasi-incompressible material behavior.[60] The isochoric part is represented by the Yeoh model[61]

$$\psi_{\text{iso}}(\boldsymbol{g};\bar{\boldsymbol{F}}) = c_1(\bar{I}_1 - 3) + c_2(\bar{I}_1 - 3)^2 + c_3(\bar{I}_1 - 3)^3, \tag{16}$$

where $2c_1 = \mu_0$ is the initial shear modulus. The anisotropic part of the free energy function

$$\psi_{\text{ani}}(\boldsymbol{g};\boldsymbol{F},\boldsymbol{f}_0) = \mu_f\langle I_4 - 1\rangle^2 \tag{17}$$

is taken as a quadratic function of the fourth invariant. This ansatz is also known as the *standard reinforcing model*.[45] The Macaulay brackets $\langle\bullet\rangle$ filter out the tensile deformations. The volumetric and anisotropic parts of the free energy function will enter the formulation at element level as constraints enforcing quasi-incompressible and quasi-inextensible behavior, whereas the isochoric part enters the formulation at Gauss quadrature points in a standard fashion.

2.2.2 | Stresses and moduli expressions

In line with (12), the Kirchoff stress expression is additively decomposed into

$$\boldsymbol{\tau} := 2\partial_{\boldsymbol{g}}\psi = \boldsymbol{\tau}^{\text{vol}} + \boldsymbol{\tau}^{\text{iso}} + \boldsymbol{\tau}^{\text{ani}}, \tag{18}$$

isotropic (which is also decomposed into volumetric and isochoric parts) and anisotropic parts. The spatial elasticity moduli establishes the relation between Lie derivative or Oldroyd rate $\pounds_{\boldsymbol{v}}\boldsymbol{\tau} = \dot{\boldsymbol{\tau}} - \boldsymbol{l}\boldsymbol{\tau} - \boldsymbol{\tau}\boldsymbol{l}^T$ of the Kirchhoff stresses and the Lie derivative of the spatial metric $\boldsymbol{g}$ via $\pounds_{\boldsymbol{v}}\boldsymbol{\tau} = \mathbb{C}\colon \pounds_{\boldsymbol{v}}\boldsymbol{g}/2$, where $\pounds_{\boldsymbol{v}}\boldsymbol{g} = (\boldsymbol{g}\boldsymbol{l} + \boldsymbol{l}^T\boldsymbol{g})$ is equivalent to the symmetric rate of deformation tensor. $\boldsymbol{l} = \dot{\boldsymbol{F}}\boldsymbol{F}^{-1}$ is the spatial velocity gradient. Within this context, the Eulerian moduli expression

$$\mathbb{C} := 4\partial^2_{\boldsymbol{g}\boldsymbol{g}}\psi(\boldsymbol{g};\boldsymbol{F},\boldsymbol{f}_0) = \mathbb{C}^{\text{vol}} + \mathbb{C}^{\text{iso}} + \mathbb{C}^{\text{ani}} \tag{19}$$

can be additively decomposed into isotropic (volumetric and isochoric) and anisotropic parts, respectively. The volumetric Kirchoff stresses read

$$\boldsymbol{\tau}^{\text{vol}} := 2\partial_{\boldsymbol{g}}\psi_{\text{vol}}(J) = p\boldsymbol{g}^{-1} \quad \text{with} \quad p := J\psi'_{\text{vol}}(J) = \frac{\kappa}{2}(J^2-1). \tag{20}$$

The Eulerian moduli expression for the volumetric part is derived as

$$\mathbb{C}^{\text{vol}} := 4\partial^2_{\boldsymbol{g}\boldsymbol{g}}U(J) = (p+\hat{\kappa})\boldsymbol{g}^{-1}\otimes\boldsymbol{g}^{-1} - 2p\mathbb{I}, \quad \text{with} \quad \hat{\kappa} = J^2\psi''_{\text{vol}}(J) = \frac{\kappa}{2}(J^2+1). \tag{21}$$

The isochoric response of the matrix can be expressed as

$$\boldsymbol{\tau}^{\text{iso}} := 2\partial_{\boldsymbol{g}}\psi_{\text{iso}}(\boldsymbol{g};\boldsymbol{F}) = \bar{\boldsymbol{\tau}} : \mathbb{P} \quad \text{with} \quad \bar{\boldsymbol{\tau}} = 2\partial_{\boldsymbol{g}}\psi_{\text{iso}}(\boldsymbol{g};\bar{\boldsymbol{F}}). \tag{22}$$

Incorporation of (22) into (16) results in

$$\boldsymbol{\tau}^{\text{iso}} = \hat{\mu}\ \text{dev}\bar{\boldsymbol{b}} \quad \text{with} \quad \hat{\mu} := 2\frac{\psi_{\text{iso}}}{\bar{I}_1} = 2\left(c_1 + 2c_2(\bar{I}_1-3) + 3c_3(\bar{I}_1-3)^2\right). \tag{23}$$

Therein, $\bar{\boldsymbol{b}} = J^{-2/3}\boldsymbol{b}$ is the unimodular part of the Finger tensor. The Eulerian moduli for the isochoric response of the matrix can be written as

$$\mathbb{C}^{\text{iso}} := 4\partial^2_{\boldsymbol{g}\boldsymbol{g}}\psi_{\text{iso}}(\boldsymbol{g};\boldsymbol{F}) = \mathbb{P} : \left[\bar{\mathbb{C}} + \frac{2}{3}(\bar{\boldsymbol{\tau}} : \boldsymbol{g})\mathbb{I} - \frac{2}{3}(\bar{\boldsymbol{\tau}}\otimes\boldsymbol{g}^{-1} + \boldsymbol{g}^{-1}\otimes\bar{\boldsymbol{\tau}})\right] : \mathbb{P}^{\text{T}}, \tag{24}$$

where $\mathbb{P}^{ab}_{cd} = [\delta^a_c\delta^b_d + \delta^a_d\delta^b_c]/2 - \delta^{ab}\delta_{cd}/3$ is the fourth-order deviatoric projection tensor. Therein,

$$\bar{\boldsymbol{\tau}} = 2\partial_{\boldsymbol{g}}\psi_{\text{iso}}(\boldsymbol{g};\bar{\boldsymbol{F}}) \quad \text{and} \quad \bar{\mathbb{C}} := 4\partial^2_{\boldsymbol{g}\boldsymbol{g}}\psi_{\text{iso}}(\boldsymbol{g};\bar{\boldsymbol{F}}) \tag{25}$$

are the Kirchoff stresses and the Eulerian moduli associated with the unimodular part of the deformation gradient. Insertion of $(25)_1$ and $(25)_2$ into (16) leads to

$$\bar{\boldsymbol{\tau}} = \hat{\mu}\bar{\boldsymbol{b}} \quad \text{and} \quad \bar{\mathbb{C}} = \hat{\mu}'\bar{\boldsymbol{b}}\otimes\bar{\boldsymbol{b}} \quad \text{with} \quad \hat{\mu}' = 8\left(c_2 + 3c_3(\bar{I}_1-3)\right). \tag{26}$$

Kirchhoff stresses generated due to the fiber reinforcement are

$$\boldsymbol{\tau}^{\text{ani}} = 2\partial_{\boldsymbol{g}}\psi_{\text{ani}}(\boldsymbol{g};\boldsymbol{F},\boldsymbol{f}_0) = 2\mu_f\langle I_4-1\rangle\boldsymbol{f}\otimes\boldsymbol{f}. \tag{27}$$

Moreover, the associated Eulerian moduli reads

$$\mathbb{C}^{\text{ani}} = 4\partial^2_{\boldsymbol{g}\boldsymbol{g}}\psi_{\text{ani}}(\boldsymbol{g};\boldsymbol{F},\boldsymbol{f}_0) = 4\mu_f\boldsymbol{f}\otimes\boldsymbol{f}\otimes\boldsymbol{f}\otimes\boldsymbol{f}. \tag{28}$$

2.2.3 | Polyconvexity of the constitutive model

The polyconvexity of hyperelastic materials and transeversely anisotropic hyperelastic materials are treated in the works of Schröder and Neff[44] and Hartmann and Neff.[62] Accordingly, the volumetric free energy function (15) is polyconvex for the physically admissible parameter domain $\kappa > 0$. The isochoric part of the free energy function (16) is polyconvex for

$$\frac{\partial^2\psi_{\text{iso}}}{\partial\bar{I}_1\partial\bar{I}_1} = 2\left(c_2 + 3c_3(\bar{I}_1 - 3.d0)\right) \geq 0 \rightarrow \boxed{c_2 \geq -3c_3(\bar{I}_1 - 3.d0)}. \tag{29}$$

This is equivalent to the statement $\hat{\mu}' \geq 0$ in Equation (26). Condition (29) is trivially satisfied for $c_2 > 0$ and $c_3 > 0$. However, the well-known s-shape stress-strain curve cannot be obtained for rubberlike materials in case $c_i > 0, i = \{1,2,3\}$. Parameter identification process of most technical rubbers gives $c_3 < 0$. In this case, the stability range of the model should be carefully checked. The anisotropic part of the free energy function is polyconvex for the physically admissible parameter domain $\mu_f > 0$.

3 | VARIATIONAL FORMULATION FOR ANISOTROPIC AND INCOMPRESSIBLE CONTINUUM

3.1 | Variational formulation for finite elasticity

The *finite elasticity* is governed by a potential functional in the form

$$\hat{\Pi}(\boldsymbol{\varphi}, t) := \hat{\Pi}^{\text{int}}(\boldsymbol{\varphi}, t) - \hat{\Pi}^{\text{ext}}(\boldsymbol{\varphi}, t), \tag{30}$$

where

$$\hat{\Pi}^{\text{int}}(\boldsymbol{\varphi}, t) := \int_{\mathscr{B}} \psi(\boldsymbol{g}, \boldsymbol{F}) dV \quad \text{and} \quad \hat{\Pi}^{\text{ext}}(\boldsymbol{\varphi}) := \int_{\mathscr{B}} \boldsymbol{\varphi} \cdot \rho_0 \bar{\boldsymbol{\gamma}} dV + \int_{\partial \mathscr{B}_t} \boldsymbol{\varphi} \cdot \bar{\boldsymbol{T}}\, dA. \tag{31}$$

For an elastic process, the energy stored in the body is defined by $\hat{\Pi}^{\text{int}}(\boldsymbol{\varphi})$, whereas $\hat{\Pi}^{\text{ext}}(\boldsymbol{\varphi})$ is the part of the work associated with the external forces. Therein, ρ_0, $\bar{\boldsymbol{\gamma}}$, and $\bar{\boldsymbol{T}}$ are the density, prescribed body force, and the surface traction, respectively. $\psi(\boldsymbol{g}, \boldsymbol{F})$ is the volume specific free energy. The boundary value problem governing finite elasticity is obtained from the elastic potential by *principle of minimum potential energy* in the variational form

$$\boldsymbol{\varphi}_t = \text{Arg} \left\{ \inf_{\boldsymbol{\varphi}_t \in \mathscr{W}} \hat{\Pi}(\boldsymbol{\varphi}, t) \right\}, \tag{32}$$

subject to Dirichlet-type boundary condition

$$\mathscr{W} = \left\{ \boldsymbol{\varphi}_t \,|\, \boldsymbol{\varphi}_t \in \mathscr{B} \quad \wedge \quad \boldsymbol{\varphi}_t = \bar{\boldsymbol{\varphi}} \quad \text{on} \quad \partial \mathscr{B}_u \right\}. \tag{33}$$

Invoking the stationarity of the potential $\hat{\Pi}(\boldsymbol{\varphi}, t)$, the variation of (32) along with localization theorem yields the *Euler-Lagrange equation*

$$1. \qquad J \,\text{div}[J^{-1}\boldsymbol{\tau}] + \rho_0 \bar{\boldsymbol{\gamma}} = 0, \tag{34}$$

leading to the balance of linear momentum for quasi-static problems in domain $\mathscr{B}$ along with Neumann-type boundary condition

$$\boldsymbol{P} \cdot \boldsymbol{N} = \boldsymbol{\tau} \cdot \boldsymbol{n} = \bar{\boldsymbol{T}} \qquad \text{on} \qquad \partial \mathscr{B}_t, \tag{35}$$

where we have made use of the identity $J\boldsymbol{F}^{-T}\boldsymbol{N}\, dA = \boldsymbol{n}\, da$, which is also known as *Nanson's formula*. $\bar{\boldsymbol{T}} = J\boldsymbol{t}$ is the scaled traction vector. The *element formulation* (*Q1* element) is derived by the consistent linearization of the weak form obtained as the first variation of (32). The weak form can be alternatively obtained from the momentum balance equation (34) by Galerkin's procedure.

3.2 | A mixed variational formulation for quasi-incompressible and quasi-inextensible continuum

The quasi-inextentensible and quasi-incompressible behavior can be enforced by enriching the minimization problem (32) by two additional penalty terms along with the decomposed representation (12)

$$\hat{\Pi}(\boldsymbol{\varphi}, p, \theta, s, \lambda) := \int_{\mathscr{B}} \pi^*(\boldsymbol{\varphi}, p, \theta, s, \lambda) dV - \hat{\Pi}^{\text{ext}}(\boldsymbol{\varphi}, t). \tag{36}$$

The mixed potential density introduced in (36) reads

$$\pi^*_{\text{int}}(\boldsymbol{\varphi}, p, \theta, s, \lambda) = \psi_{\text{iso}}(\boldsymbol{g}, \bar{\boldsymbol{F}}) + \underbrace{p(J - \theta) + \psi_{\text{vol}}(\theta)}_{\text{volumetric constraint}} + \underbrace{s(I_4 - \lambda) + \psi_{\text{ani}}(\lambda)}_{\text{inextensibility constraint}}. \tag{37}$$

Here, p, s are penalty parameters dual to the kinematic quantities θ, λ.

The motion of the body subjected to incompressible and inextensible constraints is then governed by the *mixed saddle point principle*

$$\{\boldsymbol{\varphi}_t, \theta, p, \lambda, s\} = \text{Arg} \left\{ \inf_{\boldsymbol{\varphi}_t \in \mathscr{W}} \inf_{\theta} \inf_{\lambda} \sup_{p} \sup_{s} \hat{\Pi}(\boldsymbol{\varphi}, t) \right\}, \tag{38}$$

subject to the boundary conditions $\mathscr{W} = \{\boldsymbol{\varphi}_t \,|\, \boldsymbol{\varphi}_t \in \mathscr{B} \quad \wedge \quad \boldsymbol{\varphi}_t = \bar{\boldsymbol{\varphi}} \quad \text{on} \quad \partial\mathscr{B}_u\}$. Taking the variation of (36) with respect to $\boldsymbol{\varphi}$, p, θ, s, and λ yields the weak form

$$\begin{aligned}
\delta_{\boldsymbol{\varphi}}\hat{\Pi}(\boldsymbol{\varphi}, p, \theta, s, \lambda) &= \int_{\mathscr{B}} \left\{ \left(\boldsymbol{\tau}^{\text{iso}} + pJ\boldsymbol{g}^{-1} + 2s\boldsymbol{f}\otimes\boldsymbol{f}\right) : \frac{1}{2}\pounds_{\delta\boldsymbol{\varphi}}\boldsymbol{g} \right\} dV - \delta\hat{\Pi}^{\text{ext}}(\boldsymbol{\varphi}) = 0, \\
\delta_p\hat{\Pi}(\boldsymbol{\varphi}, p, \theta, s, \lambda) &= \int_{\mathscr{B}} \delta p(J-\theta) dV = 0, \\
\delta_\theta\hat{\Pi}(\boldsymbol{\varphi}, p, \theta, s, \lambda) &= \int_{\mathscr{B}} \delta\theta\left(\psi'_{\text{vol}}(\theta) - p\right) dV = 0, \\
\delta_s\hat{\Pi}(\boldsymbol{\varphi}, p, \theta, s, \lambda) &= \int_{\mathscr{B}} \delta s(I_4 - \lambda) dV = 0, \\
\delta_\lambda\hat{\Pi}(\boldsymbol{\varphi}, p, \theta, s, \lambda) &= \int_{\mathscr{B}} \delta\lambda\left(\psi'_{\text{ani}}(\lambda) - s\right) dV = 0,
\end{aligned} \tag{39}$$

from which the mixed finite element method can be constructed. Therein, $\pounds_{\delta\boldsymbol{\varphi}}\boldsymbol{g}$ is the Lie derivative of the current metric along the variation $\delta\boldsymbol{\varphi}$. Taking the variation of the potential density (37), *Euler-Lagrange equations* of the mixed variational principle read

$$\begin{aligned}
&1. \quad J\text{div}[J^{-1}\boldsymbol{\tau}] + \rho_0\bar{\boldsymbol{\gamma}} &&= 0 \\
&2. \quad J - \theta &&= 0 \\
&3. \quad \psi'_{\text{vol}}(\theta) - p &&= 0 \\
&4. \quad I_4 - \lambda &&= 0 \\
&5. \quad \psi'_{\text{ani}}(\lambda) - s &&= 0,
\end{aligned} \tag{40}$$

along with the Neumann-type boundary conditions $\mathscr{W}_t = \{\boldsymbol{\sigma}\cdot\boldsymbol{n} = \boldsymbol{t} \quad \text{on} \quad \partial\mathscr{B}_t\}$.

3.3 | Consistent linearization of the mixed potential

It can be shown that $\frac{1}{2}\pounds_{\delta\boldsymbol{\varphi}}\boldsymbol{g} = \text{sym}(\boldsymbol{g}\nabla_x\delta\boldsymbol{\varphi})$. Equation (39.1) is nonlinear in terms of $\boldsymbol{\varphi}$ and Equations (39.2-5) act as additional constraints on (39.1). Consistent linearization of (39.1) around $\boldsymbol{\varphi}$ yields

$$\begin{aligned}
D\delta_{\boldsymbol{\varphi}}\hat{\Pi}\cdot\Delta\boldsymbol{\varphi} = &\int_{\mathscr{B}} \boldsymbol{g}\nabla_x\delta\boldsymbol{\varphi} : \left\{\nabla_{\boldsymbol{x}}\Delta\boldsymbol{\varphi}\left(\boldsymbol{\tau}^{\text{iso}} + pJ\boldsymbol{g}^{-1} + 2s\boldsymbol{f}\otimes\boldsymbol{f}\right)\right\} dV \\
&+ \int_{\mathscr{B}} \boldsymbol{g}\nabla_x\delta\boldsymbol{\varphi} : \left\{pJ\mathbb{V} + \mathbb{C}^{\text{iso}}\right\} : \boldsymbol{g}\nabla_x\Delta\boldsymbol{\varphi}\, dV \\
&+ \int_{\mathscr{B}} \boldsymbol{g}\nabla_x\delta\boldsymbol{\varphi} : J\Delta p\boldsymbol{g}^{-1} dV. + \int_{\mathscr{B}} \boldsymbol{g}\nabla_x\delta\boldsymbol{\varphi} : 2\Delta s\boldsymbol{f}\otimes\boldsymbol{f}\, dV,
\end{aligned} \tag{41}$$

with the following definition:

$$\mathbb{V} = \boldsymbol{g}^{-1}\otimes\boldsymbol{g}^{-1} - 2\mathbb{I}_{\boldsymbol{g}^{-1}}, \tag{42}$$

where ${\mathbb{I}_{\boldsymbol{g}^{-1}}}^{abcd} = (\delta^{ac}\delta^{bd} + \delta^{ad}\delta^{bc})/2$ is the fourth-order symmetric identity map. Therein, we have made use of the identity $\frac{1}{2}\pounds_{\Delta\boldsymbol{\varphi}}\boldsymbol{g} = \text{sym}(\boldsymbol{g}\nabla_x\Delta\boldsymbol{\varphi})$, where $\pounds_{\Delta\boldsymbol{\varphi}}\boldsymbol{g}$ is the Lie derivative of the current metric along the increment $\Delta\boldsymbol{\varphi}$. The first equation in (39) is equivalent to the balance of linear momentum for quasi-static problems and (39.2-5) are the constraints enforcing the incompressibility and inextensibility, respectively. The constraint equations will be enforced weakly in an integral sense within subdomains $\mathscr{B}_e$ such that $\mathscr{B}_0 \approx \bigcup_{e=1}^{n_e}\mathscr{B}_e$, with n_e denoting the number of the subdomains $\mathscr{B}_e$ in the body. The penalty parameter p and the kinematical variable θ can be discretized consistent with (39.2) and (39.3) within the subdomain $\mathscr{B}_e$ in the following sense:

$$\bar{\theta} = \frac{1}{V^e}\int_{\mathscr{B}_e} J\, dV, \qquad \bar{p} = \frac{1}{V^e}\int_{\mathscr{B}_e} \psi'_{\text{vol}}(\theta)\, dV = \psi'_{\text{vol}}(\bar{\theta}). \tag{43}$$

This proposal yields a constant value for $\bar{\theta}$ and $\bar{p}$. With the definitions (43.1) and (43.2), $\bar{\theta}$ and $\bar{p}$ can be physically interpreted as the mean dilatation and the mean negative pressure over the element domain, respectively. The incremental

form of the mean negative pressure $\bar{p}$ takes the form

$$\Delta\bar{p} = \psi''_{\text{vol}}(\bar{\theta})\Delta\bar{\theta}, \quad \text{where} \quad \Delta\bar{\theta} = \frac{1}{V^e}\int_{\mathscr{B}_e} J\boldsymbol{g}^{-1} : \boldsymbol{g}\nabla_x\Delta\boldsymbol{\varphi}\, dV. \tag{44}$$

In a similar way, the penalty parameter s and the kinematical variable λ can be discretized consistent with (39.4) and (39.5) within the subdomain $\mathscr{B}_e$ in the following sense:

$$\bar{\lambda} = \frac{1}{V^e}\int_{\mathscr{B}_e} I_4\, dV \quad \text{and} \quad \bar{s} = \frac{1}{V^e}\int_{\mathscr{B}_e} \psi'_{\text{ani}}(\lambda)\, dV \approx \psi'_{\text{ani}}(\bar{\lambda}). \tag{45}$$

This proposal yields a constant value for $\bar{\lambda}$ and $\bar{s}$. With the definitions (45.1) and (45.2), $\bar{\lambda}$ and $\bar{s}$ can be physically interpreted as the mean fiber stretch and the mean fiber stress over the element domain, respectively. The incremental form of the mean fiber stress $\bar{s}$ takes the form

$$\Delta\bar{s} = \psi''_{\text{ani}}(\bar{\lambda})\Delta\bar{\lambda}, \quad \text{where} \quad \Delta\bar{\lambda} = \frac{1}{V^e}\int_{\mathscr{B}_e} 2\boldsymbol{f}\otimes\boldsymbol{f} : \boldsymbol{g}\nabla_x\Delta\boldsymbol{\varphi}\, dV. \tag{46}$$

The stresses and the moduli expressions can be redefined as

$$\hat{\boldsymbol{\tau}} = \boldsymbol{\tau}^{\text{iso}} + \bar{p}J\boldsymbol{g}^{-1} + 2\bar{s}\boldsymbol{f}\otimes\boldsymbol{f} \qquad \hat{\mathbb{C}} = \bar{p}J\mathbb{V} + \mathbb{C}^{\text{iso}}. \tag{47}$$

Now, substituting (44), (46)), and (47) into (41) and exploiting the symmetry of $\hat{\boldsymbol{\tau}}$ and $\hat{\mathbb{C}}$, we reach the final expression for the linearized term

$$\begin{aligned} D\delta_{\boldsymbol{\varphi}}\hat{\Pi}\cdot\Delta\boldsymbol{\varphi} = \mathop{\mathsf{A}}_{e=1}^{n}\Bigg\{ &\int_{\mathscr{B}_e} \boldsymbol{g}\nabla_x\delta\boldsymbol{\varphi} : \nabla_{\boldsymbol{x}}\Delta\boldsymbol{\varphi}\,\hat{\boldsymbol{\tau}}\, dV + \int_{\mathscr{B}_e} \boldsymbol{g}\nabla_x\delta\boldsymbol{\varphi} : \hat{\mathbb{C}} : \boldsymbol{g}\nabla_x\Delta\boldsymbol{\varphi}\, dV \\ &+ \int_{\mathscr{B}_e} J\boldsymbol{g}\nabla_x\delta\boldsymbol{\varphi} : \boldsymbol{g}^{-1}\, dV\, \psi''_{\text{vol}}(\bar{\theta})\frac{1}{V^e}\int_{\mathscr{B}_e} J\boldsymbol{g}\nabla_x\Delta\boldsymbol{\varphi} : \boldsymbol{g}^{-1}\, dV \\ &+ \int_{\mathscr{B}_e} \boldsymbol{g}\nabla_x\delta\boldsymbol{\varphi} : 2\boldsymbol{f}\otimes\boldsymbol{f}\, dV\, \psi''_{\text{ani}}(\bar{\lambda})\frac{1}{V^e}\int_{\mathscr{B}_e} \boldsymbol{g}\nabla_x\Delta\boldsymbol{\varphi} : 2\boldsymbol{f}\otimes\boldsymbol{f}\, dV\Bigg\}. \end{aligned} \tag{48}$$

4 | FINITE ELEMENT FORMULATION

4.1 | Element discretization

In the final step, we perform the spatial discretization of the field variables to obtain algebraic counterparts of the residual expression (39.1) and construct the element matrices from the linearized term (48). The trilinear interpolation is adopted for the placement $\boldsymbol{\varphi}$, whereas the mean values of the negative pressure $\bar{p}$, dilatation, $\bar{\theta}$ fiber stress $\bar{s}$, and fiber stretch $\bar{\lambda}$ are taken as constant through the element (see Figure 4). Then, the field variables and the associated weight functions are interpolated through each element domain by introducing the discrete nodal values and $\mathscr{C}^0$-continuous shape functions

$$\boldsymbol{\varphi}^h = \sum_{I=1}^{\text{n}_{\text{en}}} \mathcal{N}^I\,\hat{\boldsymbol{x}}_I, \quad \delta\boldsymbol{\varphi}^h = \sum_{I=1}^{\text{n}_{\text{en}}} \mathcal{N}^I\,\delta\hat{\boldsymbol{x}}_I, \quad \Delta\boldsymbol{\varphi}^h = \sum_{I=1}^{\text{n}_{\text{en}}} \mathcal{N}^I\,\Delta\hat{\boldsymbol{x}}_I, \tag{49}$$

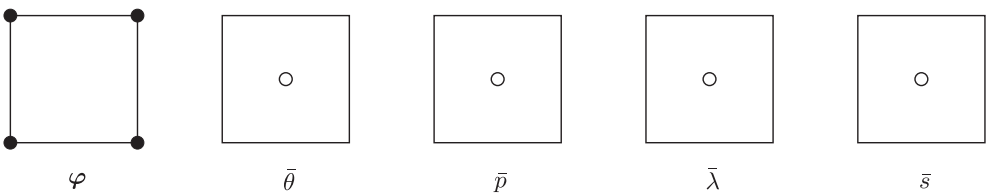

FIGURE 4 Extended *Q1P0F0* mixed finite element design for quasi-incompressible and quasi-inextensible hyperelasticity. For the sake of convenience, the sketch is two dimensional

where n_{en} refers to the number of nodes per element. Based on the discretization (49), the spatial gradient of the weight functions and of the incremental fields read

$$\nabla_x(\delta\boldsymbol{\varphi}^h) = \sum_{I=1}^{n_{en}} \delta\hat{\boldsymbol{x}}_I \otimes \nabla_x \mathcal{N}^I, \quad \nabla_x \Delta\boldsymbol{\varphi}^h = \sum_{I=1}^{n_{en}} \Delta\hat{\boldsymbol{x}}_I \otimes \nabla_x \mathcal{N}^I. \tag{50}$$

Incorporating the discretized representations (49), (50) in (39), we obtain the discrete residual vector

$$\mathbb{R}^{\varphi} = \mathop{\mathsf{A}}_{e=1}^{n_{el}} \sum_{I=1}^{n_{en}} \int_{\mathscr{B}_e^h} \left[\nabla_x \mathcal{N}^I \cdot \hat{\boldsymbol{\tau}} - \mathcal{N}^I \rho_0 \bar{\boldsymbol{\gamma}}\right] dV - \mathop{\mathsf{A}}_{e=1}^{n_{el}^s} \sum_{I=1}^{n_{en}^s} \int_{\partial\mathcal{S}_t^e} \mathcal{N}^I \bar{\boldsymbol{T}}\, dA = \boldsymbol{0}, \tag{51}$$

where the operator A denotes the standard assembly of element contributions at the local element nodes $I = 1, \ldots, n_{en}$ over n_{el} subdomains.

Following analogous steps, the discrete form of the residual term (39.1) can readily be obtained by substituting the discretized representations (49)-(50). The linearization of the discrete residual expressions (51.1-3) can be shown as follows:

$$\text{Lin}\, \mathbb{R}^{\varphi} = \mathbb{R}^{\varphi} + \frac{\partial \mathbb{R}^{\varphi}}{\partial \mathbb{U}} \Delta\mathbb{U}, \quad \mathbb{U} = \mathop{\mathsf{A}}_{e=1}^{n_{el}} \hat{\boldsymbol{x}}^h. \tag{52}$$

The element matrix is derived via incorporation of (49), (50) into (48)

$$\mathbb{K} = \frac{\partial \mathbb{R}^{\varphi}}{\partial \mathbb{U}} = \mathop{\mathsf{A}}_{e=1}^{n_{el}} \mathbb{K}_{el}, \tag{53}$$

where the element stiffness matrix can be expressed in terms of

$$\mathbb{K}_{el} = \mathbb{K}_{el}^{\text{mat}} + \mathbb{K}_{el}^{\text{geo}} + \mathbb{K}_{el}^{\text{vol}} + \mathbb{K}_{el}^{\text{ani}} \tag{54}$$

material, geometric, volumetric, and anisotropic contributions, respectively. With the help of the element-average quantities

$$\nabla_x \bar{\mathcal{N}}^I = \int_{\mathscr{B}_{el}^h} J\, \nabla_x \mathcal{N}^I\, dV, \qquad \nabla_x \bar{\mathcal{F}}^I = \int_{\mathscr{B}_{el}^h} \nabla_x \mathcal{N}^I : \boldsymbol{f} \otimes \boldsymbol{f}\, dV, \tag{55}$$

we define the contributions to the element stiffness matrix as follows:

$$\begin{aligned}
\mathbb{K}_{el}^{\text{mat}\,IJ} &= \int_{\mathscr{B}_{el}^h} \nabla_x^T \mathcal{N}^I \cdot \hat{\mathbb{C}} \cdot \nabla_x \mathcal{N}^J dV, \quad \mathbb{K}_{el}^{\text{vol}\,IJ} = \nabla_x^T \bar{\mathcal{N}}^I \frac{\psi''_{\text{vol}}(\bar{\theta})}{V_e} \nabla_x \bar{\mathcal{N}}^J, \\
\mathbb{K}_{el}^{\text{geo}\,IJ} &= \int_{\mathscr{B}_{el}^h} \nabla_x \mathcal{N}^I \cdot \hat{\boldsymbol{\tau}} \cdot \nabla_x \mathcal{N}^J dV, \quad \mathbb{K}_{el}^{\text{ani}\,IJ} = \nabla_x^T \bar{\mathcal{F}}^I \frac{\psi''_{\text{ani}}(\bar{\lambda})}{V_e} \nabla_x \bar{\mathcal{F}}^J.
\end{aligned} \tag{56}$$

The algorithmic box for the *Q1P0F0* element is summarized in Table 1. In the sequel, the finite element implementation specific to eight-noded brick element will be presented. To this end, the shape functions can be defined for an eight-noded brick element

$$\mathcal{N}^I(\boldsymbol{\xi}) = \frac{1}{8}\left(1 + \xi_1\xi_1^I\right)\left(1 + \xi_2\xi_2^I\right)\left(1 + \xi_3\xi_3^I\right), \tag{57}$$

with the nodal values of

$$\begin{aligned}
\xi_1^I &= [-1\,+1\,+1\,-1\,-1\,+1\,+1\,-1] \\
\xi_2^I &= [-1\,-1\,+1\,+1\,-1\,-1\,+1\,+1] \\
\xi_3^I &= [-1\,-1\,-1\,-1\,+1\,+1\,+1\,+1]
\end{aligned} \tag{58}$$

for a cube in the parametric space, as shown in Figure 5. For the computation of spatial gradients with respect to Lagrangian and Eulerian coordinates, the following maps will be defined.

5 | REPRESENTATIVE NUMERICAL EXAMPLES

In this section, the performance of the proposed mixed-element formulation will be demonstrated through three boundary value problems. In the first two examples, the performance of the proposed *Q1P0F0* element will be demonstrated for

TABLE 1 Flowchart for the computation of *Q1P0F0* element stiffness matrix

a) Volumetric part of the stiffness matrix:

Mean dilatation $\bar{\theta}$, negative pressure $\bar{p}$, mean fiber stretch $\bar{\lambda}$, and mean fiber stress $\bar{s}$ will be computed.

{ LOOP $[\alpha = 1, 8]$ Given: current position $\hat{\boldsymbol{x}}^h = \hat{\boldsymbol{u}}^h + \hat{\boldsymbol{X}}^h$, shape functions $\mathcal{N}(\boldsymbol{\xi}) := \mathcal{N}^I(\boldsymbol{\xi})$

Set: $V^e = v^e = 0 \bar{\lambda} = 0$

1. Compute shape functions, derivative of the shape function in parametric space and transformation map at $\boldsymbol{\xi}(\alpha)$

$$\mathcal{N}(\boldsymbol{\xi}), \quad \nabla_{\xi i}\mathcal{N}(\boldsymbol{\xi}), \quad \text{and} \quad \boldsymbol{J} = \nabla_{\xi}\mathcal{N}\hat{\boldsymbol{X}}^h \quad \text{at} \quad \boldsymbol{\xi} = \boldsymbol{\xi}(\alpha)$$

2. Compute the material and spatial derivative of shape functions, and deformation gradient

$$\nabla_X \mathcal{N} = \nabla_{\xi}\mathcal{N}\boldsymbol{J}^{-1}, \quad \boldsymbol{F} = \nabla_X \mathcal{N}\hat{\boldsymbol{x}}, \quad \text{and} \quad \nabla_x \mathcal{N} = \nabla_X \mathcal{N}\boldsymbol{F}^{-1}$$

3. Compute the initial and current element volume and the integrate the fiber stretch $\boldsymbol{f} = \boldsymbol{F}\boldsymbol{f}_0$

$$V^e \leftarrow V^e + \det \boldsymbol{J} w_\alpha \qquad v^e \leftarrow v^e + \det \boldsymbol{J} \det \boldsymbol{F} w_\alpha$$
$$\lambda = \boldsymbol{f} \cdot \boldsymbol{g}\boldsymbol{f} \qquad \bar{\lambda} \leftarrow \bar{\lambda} + \lambda \det \boldsymbol{J} w_\alpha$$

4. Compute $\nabla_x \bar{\mathcal{N}} := \nabla_x \bar{\mathcal{N}}^I$ and $\nabla_x \bar{\mathcal{F}} := \nabla_x \bar{\mathcal{F}}^I$

$$\nabla_x \bar{\mathcal{N}} \leftarrow \nabla_x \bar{\mathcal{N}} + \det \boldsymbol{J} \det \boldsymbol{F} w_\alpha \nabla_x \mathcal{N} \qquad \nabla_x \bar{\mathcal{F}} \leftarrow \nabla_x \bar{\mathcal{F}} + \det \boldsymbol{J} w_\alpha \nabla_x \mathcal{N} : \boldsymbol{f} \otimes \boldsymbol{f} \quad \}$$

5. Compute $\bar{\theta}$, $\bar{p}$, $\bar{\lambda}$, and $\bar{s}$

$$\bar{\theta} = \frac{v^e}{V^e} \qquad \bar{p} = \psi'_{\text{vol}}(\bar{\theta}) \qquad \bar{\lambda} \leftarrow \frac{\bar{\lambda}}{V^e} \qquad \bar{s} = \psi'_{\text{ani}}(\bar{\lambda})$$

6. Compute $\boldsymbol{K}_{\text{vol}}$ and $\boldsymbol{K}_{\text{iso}}$

$$K_{\text{vol}}^{3(I-1)+i,3(J-1)+j} = (\bar{\mathcal{N}}_{,x})_i^I \frac{\psi''_{\text{vol}}(\bar{\theta})}{V^e} (\bar{\mathcal{N}}_{,x})_j^J$$
$$K_{\text{ani}}^{3(I-1)+i,3(J-1)+j} = (\bar{\mathcal{F}}_{,x})_i^I \frac{\psi''_{\text{ani}}(\bar{\lambda})}{V^e} (\bar{\mathcal{F}}_{,x})_j^J$$

b) Material and geometric part of the stiffness matrix:

{ LOOP $[\alpha = 1, 8]$

7. Compute $\boldsymbol{K}_{\text{mat}}$ and $\boldsymbol{K}_{\text{geo}}$

$$K_{\text{geo}}^{3(I-1)+a,3(J-1)+a} = K_{\text{geo}} + (\mathcal{N}_{,x})_i^I (\mathcal{N}_{,x})_j^J \tau^{ij} \det \boldsymbol{J} w_\alpha$$
$$K_{\text{mat}}^{3(I-1)+i,3(J-1)+k} = K_{\text{mat}} + (\mathcal{N}_{,x})_j^I \hat{\mathbb{C}}^{ijkl} (\mathcal{N}_{,x})_l^J \det \boldsymbol{J} w_\alpha \quad \}$$

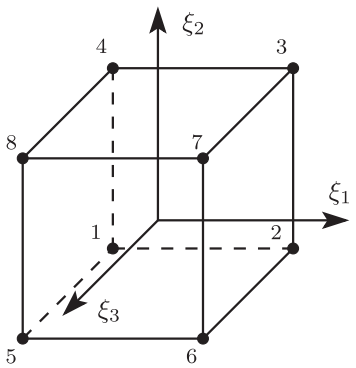

FIGURE 5 Unit cube in the parameter space. Local coordinates are defined by $\boldsymbol{\xi} \in \mathcal{A}$, where $\mathcal{A} := \{\boldsymbol{\xi} \in \mathbb{R}^3 \mid -1 \le \xi_i \le +1; \quad i = 1, 3\}$

inflation and torsion conditions, whereas the third example will be used for comparison with standard displacement *Q1* and mixed displacement-pressure formulation *Q1P0*, respectively. The mixed element formulation outlined in Section 3 is implemented into general purpose open source finite element program *FEAP*.

5.1 | Isochoric uniaxial tension test

In order to validate the element formulations used throughout the investigations, an isochoric uniaxial tension test is carried out with *Q1*, *Q1P0*, and *Q1P0F0* elements with a unit cube discretized with single element. The material parameters for the baseline neo-Hookean solid are taken as $\mu = 2c_1 = 1$ MPa, $c_2 = c_3 = 0$, and $\mu_f = 100$ MPa. In the exact incompressible limit, the volumetric part does not play a role and the pressure expression can be derived from the equilibrium conditions $-p = \sigma_{22} = \sigma_{22}$. Consequently, the analytical solution for the isochoric uniaxial tension deformation in the

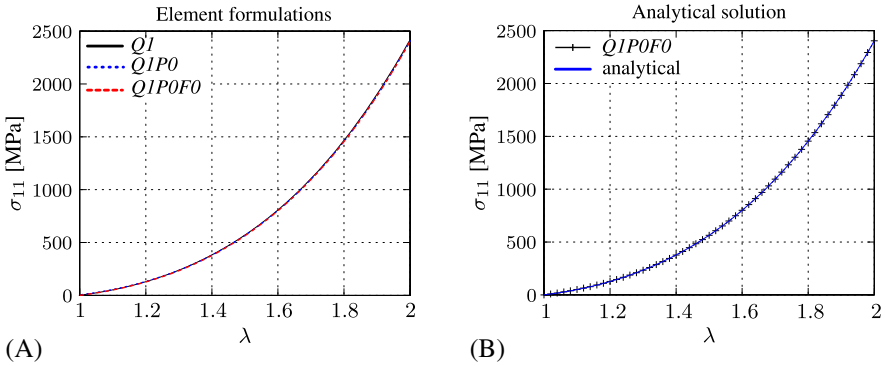

FIGURE 6 Isochoric uniaxial tension test. A, comparison of the results for *Q1*, *Q1P0*, and *Q1P0F0* element formulation; B, comparison of the results for the analytical solution and the *Q1P0F0* element formulation [Colour figure can be viewed at wileyonlinelibrary.com]

fiber orientation direction can be derived as

$$\sigma_{11} = \mu \left[\lambda - \frac{1}{\sqrt{\lambda}} \right] + 2\mu_f (\lambda^2 - 1)\lambda^2 . \tag{59}$$

The results obtained from *Q1*, *Q1P0*, and *Q1P0F0* elements and the analytical results are depicted in Figure 6. All three formulations give identical results with the analytical solution.

5.2 | Inflation of a hollow circular

A hollow cylinder is inflated monotonically with a pressure $\hat{p}(t) = 0.1t$ [MPa], where t is the time in seconds. The geometry and the mesh of the problem are depicted in Figure 7. The fibers are aligned in the vertical z-direction and the tube is fixed against motion in all directions at the bottom and top surfaces. Due to symmetry, only half of the geometry is modeled along with the boundary conditions depicted in Figure 7. The material parameters for the unidirectionally reinforced Yeoh model are given in Table 2.

The deformed shape at various stages of loading are depicted in Figure 8 along with contour plots for the true radial stresses σ_r. The incremental time step is taken as $\Delta t = 0.5$ s throughout the simulation. The simulations show quadratic convergence, where the norm of the residual vector normalized with respect to the first residual norm is shown in Table 3. The stability of the material model is checked according to Equation (29). Throughout the simulation, the deformation state is well below the critical limit $c_2 \geq -3c_3(\bar{I}_1 - 3.d0)$ and the constitutive model remains polyconvex.

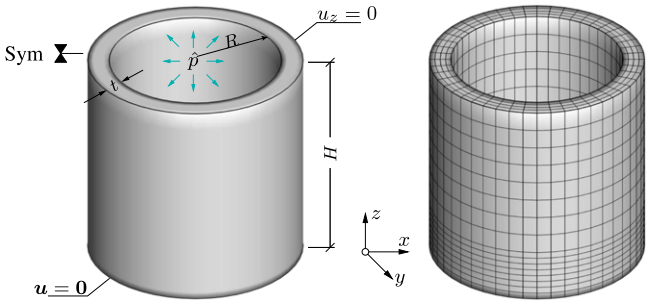

FIGURE 7 Geometry and mesh. A hollow cylinder with dimensions $H \times R \times t = 200 \times 100 \times 20$ mm is fixed at both ends and subjected to a monotonically increasing internal pressure p. Due to symmetry, only half of the hollow cylinder is discretized with $16 \times 48 \times 4$ eight-noded brick elements [Colour figure can be viewed at wileyonlinelibrary.com]

TABLE 2 Material parameters used during the inflation of hollow cylinder

Parameter	Value	Unit	Parameter	Value	Unit
κ	0.5×10^3	[MPa]	$\mu = 2c_1$	0.5	[MPa]
c_2	0.2	[MPa]	c_3	-0.541×10^{-2}	[MPa]
μ_f	0.5×10^3	[MPa]	$\boldsymbol{f}_0$	[0, 0, 1]	[–]

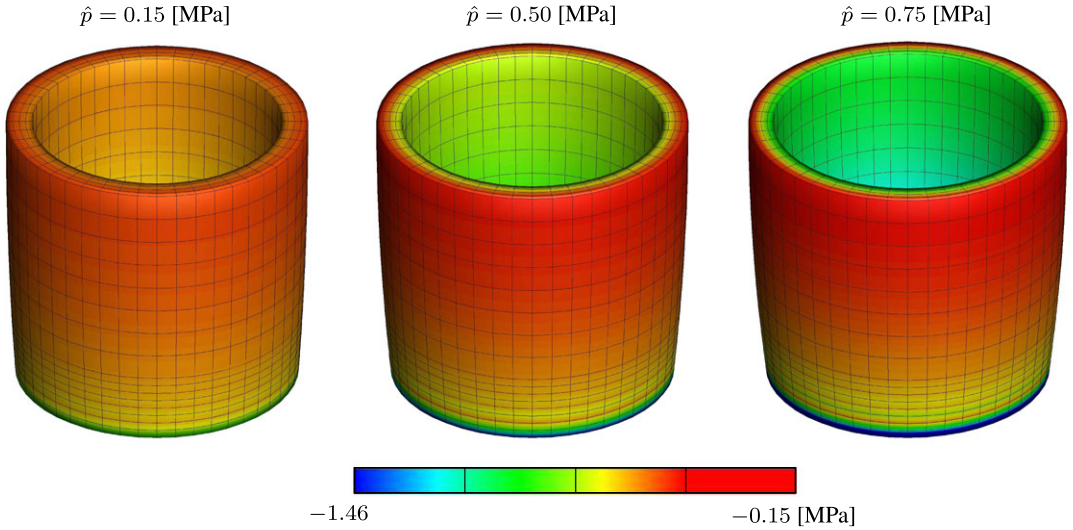

FIGURE 8 The radial stress σ_r depicted on deformed mesh for pressure levels $\hat{p} = 0.15$, $\hat{p} = 0.50$, and $\hat{p} = 0.75$ MPa, respectively

TABLE 3 Convergence of the mixed-element formulation for inflation of a hollow cylinder example

Time [s]	2.5	5	7.5	10	15	30
Step 1	1.0000E+00	1.0000E+00	1.0000E+00	1.0000E+00	1.0000E+00	1.0000E+00
Step 2	3.9995E+01	1.1712E+00	6.1647E−01	3.9924E−01	2.2121E−01	8.4379E−02
Step 3	4.7022E−02	3.5609E−03	9.0674E−04	3.6388E−04	1.0859E−04	1.6588E−05
Step 4	3.7037E−05	1.2247E−07	5.8225E−09	7.4148E−10	4.6832E−11	1.1527E−11
Step 5	8.9617E−12	6.2114E−12	–	–	–	–
nsteps	5	5	4	4	4	4

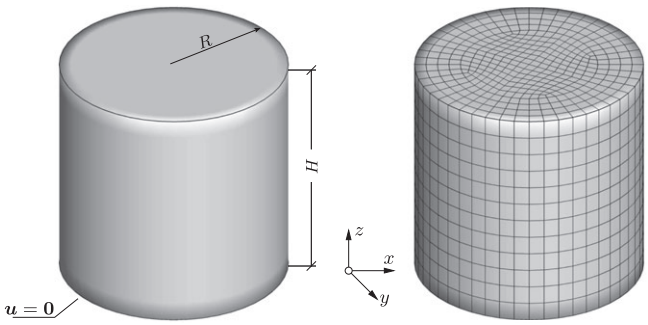

FIGURE 9 Geometry and mesh. A solid cylinder block with dimensions $H \times R \times t = 200 \times 100 \times 20$ mm is fixed at top $z = H$ and bottom $z = 0$ surfaces and the top surface is subjected to a rotation about z-axis. The cylinder block is discretized with 12×384 eight-noded brick elements

5.3 | Torsion of a circular cylinder

In the second example, a fiber reinforced rubber cylinder is subjected to a twist around z-axis. The geometry of the specimen is depicted in Figure 9. The bottom $z = 0$ and top $z = H$ surfaces are fixed and the top surface is rotated around the center monotonically. The material parameters are due to Table 2. The material parameters are chosen in such a way that the inextensibility and incompressibility constraints are of the same order of magnitude. The solid cylinder block is discretized with 12×384 eight-noded brick elements. In Figure 10, the deformed shape and the tangential stress σ_t are depicted for top rotations, corresponding to $\theta_z = \pi/6$, $\theta_z = \pi/3$, and $\theta_z = \pi/2$ radians, respectively. In the absence of the fibers, the macroscopic loading will lead to isochoric deformations everywhere. In the current example, however, a competition occurs between inextensibility and incompressibility constraints. Under pure isochoric

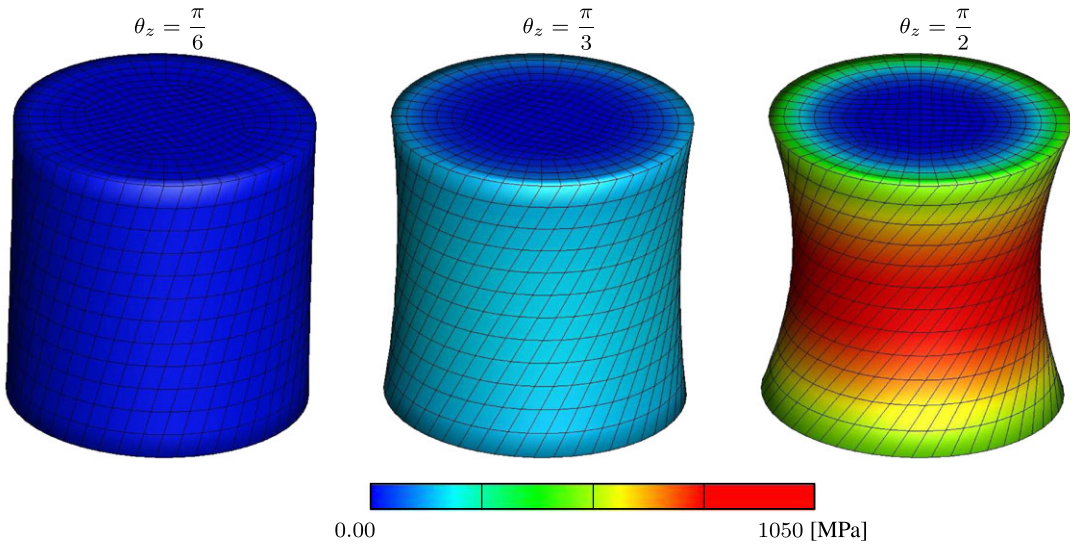

FIGURE 10 The tangential stress σ_t depicted on deformed mesh top surface rotation corresponding to $\theta_z = \pi/6$, $\theta_z = \pi/3$, and $\theta_z = \pi/2$ radians, respectively

TABLE 4 Convergence of the mixed-element formulation for torsion of a solid cylinder example

Time [s]	5	15	30	45	60	90
Step 1	1.0000E+00	1.0000E+00	1.0000E+00	1.0000E+00	1.0000E+00	1.0000E+00
Step 2	3.8286E+00	1.0879E−02	4.2015E−03	2.6205E−03	1.9078E−03	1.3414E−03
Step 3	1.5038E+00	2.5032E−03	2.2519E−04	5.8615E−05	2.4878E−05	9.8452E−06
Step 4	1.3486E−01	1.6467E−06	1.8309E−07	6.7850E−08	7.5299E−08	2.5396E−08
Step 5	1.1811E−03	2.1253E−10	7.8760E−12	1.1783E−12	3.7898E−13	4.7672E−13
nsteps	7	5	5	5	5	5

deformations, very high stresses are generated due to the stiff fibers, enforcing the neck-type thinning in the midsection as an energetically more favorable state, see Figure 10. On the numerical side, excellent convergence behavior of the quasi-incompressible/-inextensible element formulation documented in Table 4, where the norm of the residual vector normalized with respect to the first residual norm is given in tabular form. The incremental time step is taken as $\Delta t = 5$ s throughout the simulation and the rotation rate is taken as $\dot{\theta}_z = 5°/\text{s}$.

5.4 | Dual clamped patch test

This numerical example has been recently proposed by Schröder et al.[55] A square block of unit dimensions 1×1 is clamped at top and bottom surfaces and it is subjected to a distributed loading $q_0 = 30$ (see Figure 11). The fiber direction $\boldsymbol{f}_0 = [0.5, \sqrt{3}/2, 0]$ is kept constant and the fiber stiffness μ_f is varied $\mu_f = \{10^2, 10^4, 10^6, 10^8\}$ to study the stability of the proposed formulation toward inextensibility limit. The proposed formulation is compared to the standard linear

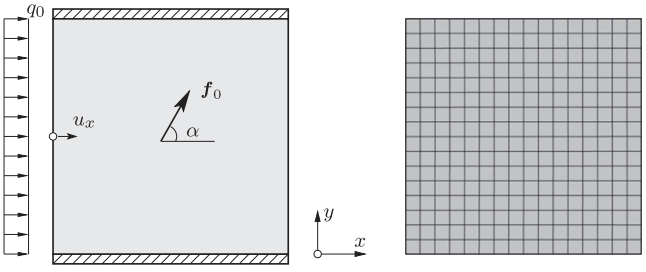

FIGURE 11 Dual clamped patch test. A solid square block with unit dimensions 1×1 is fixed at top $y = 1$ and bottom $y = 0$ surfaces and the side surface $x = 0$ is subjected to normal traction $q_0 = 30$. The fibers are aligned $\alpha = 60°$ from the horizontal plane. The cylinder block is discretized with $n \times n$ brick elements, where $n = \{2, 4, 8, 16, 32, 64\}$

displacement element *Q1* formulation and the mean dilatation approach denoted as *Q1P0* formulation. The specimen is monotonically loaded via $q(t) = q_o t$. Initially, the time increment is taken as $\Delta t = 1$. If the global Newton-Raphson algorithm does not converge within 15 time steps, the time increment is halved and the simulation is restarted from $t = 0$. The process is continued until $\Delta t \to 1/512$ is reached. Unlike the original problem suggested in the aforementioned work,[55] the free energy function for the isotropic part is taken as the neo-Hookean model based on the isochoric-volumetric split

$$\psi_{\text{iso}}(\boldsymbol{g}; \bar{\boldsymbol{F}}) = \frac{\mu}{2}(\bar{I}_1 - 3) \quad \text{and} \quad \psi_{\text{vol}}(J) = \frac{\kappa}{4}\left(J^2 - 2\ln J - 1\right), \tag{60}$$

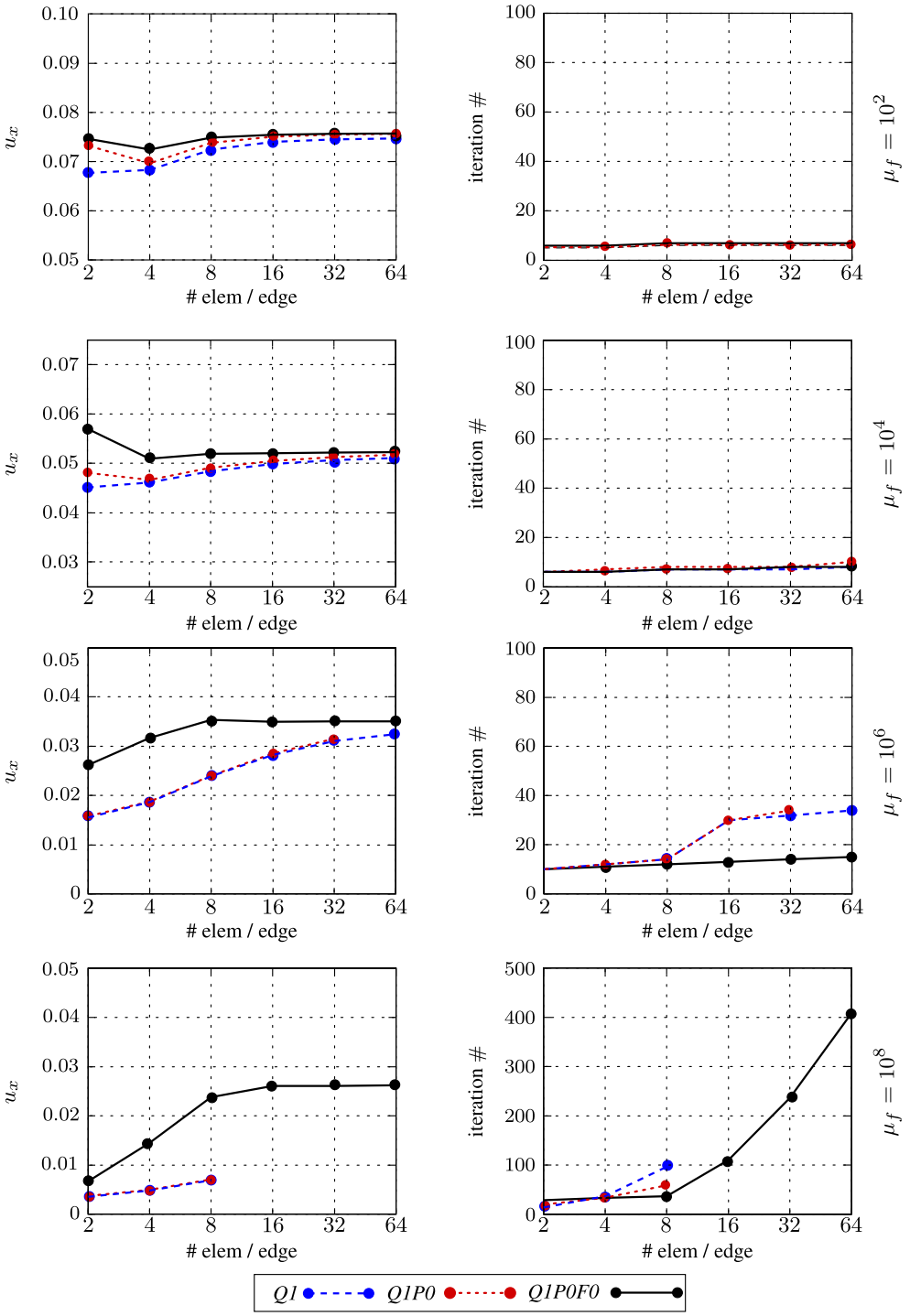

FIGURE 12 Dual clamped patch test with $\nu = 0.3$. Comparison of the *Q1*, *Q1P0*, and *Q1P0FO* element formulations for fiber stifness values $\mu_f = \{10^2, 10^4, 10^6, 10^8\}$ [Colour figure can be viewed at wileyonlinelibrary.com]

inline with the *Q1P0* formulation. In the first set of analysis, the initial Poisson ratio is set to $\nu = 0.3$, which led to the material parameters $\mu = 76.9231$ and $\kappa = 166.667$ for initial elasticity modulus $E = 200$. In the second set of analysis, the material parameters are taken as $\mu = 67.11409$ and $\kappa = 3333.333$, corresponding to the initial Poisson ratio $\nu = 0.49$, which mimics the quasi-incompressible limit. Moreover, as an extreme case, a third simulation is carried out with the material parameters are taken as $\mu = 66.6711$ and $\kappa = 333333.3333$, corresponding to the initial Poisson ratio $\nu = 0.4999$. For the analysis, six sets of mesh densities are used, where the number of elements per edge are varied as $n = \{2, 4, 8, 16, 32, 64\}$. The original problem is two dimensional. The current formulation is reduced to two-dimensional

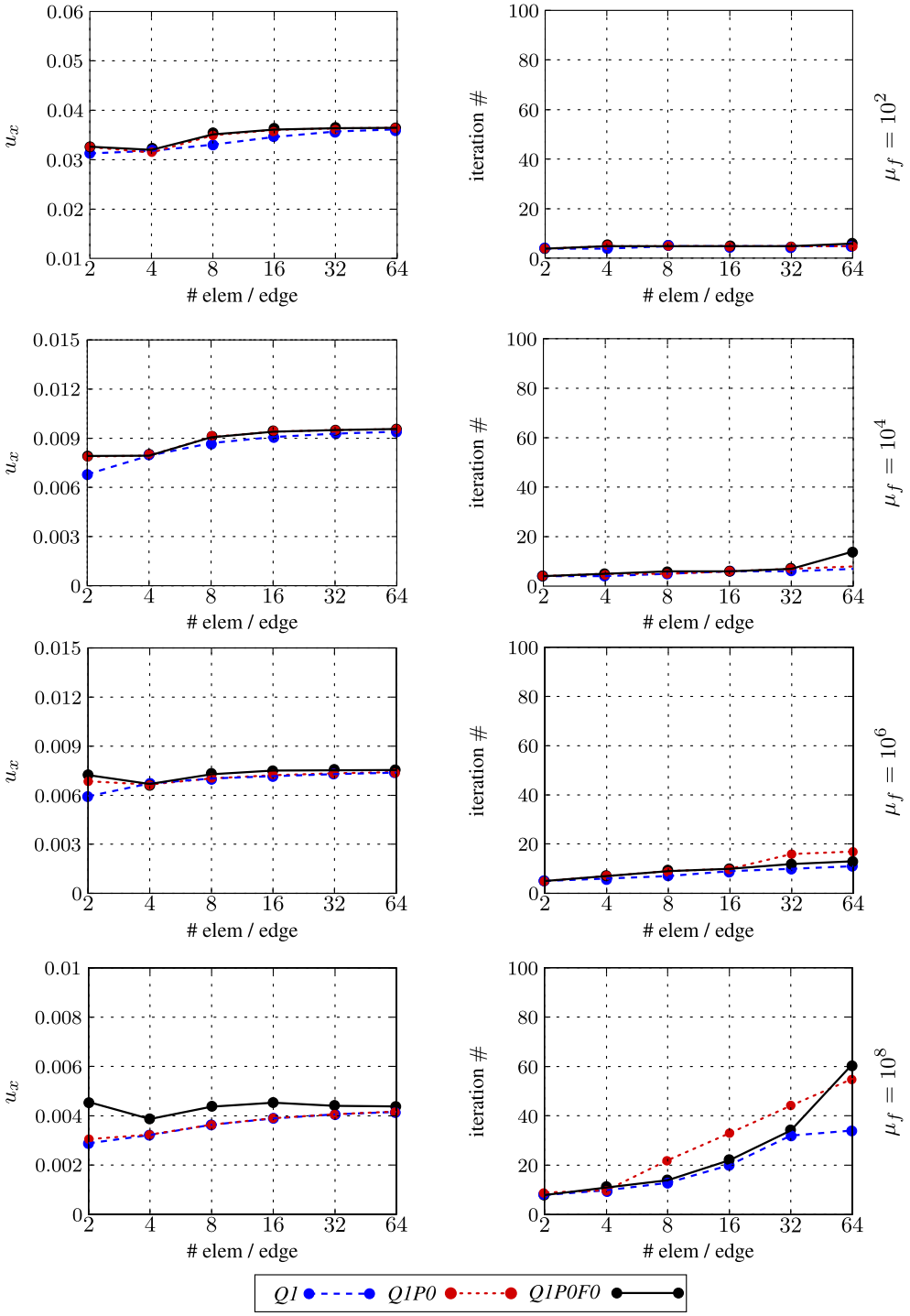

FIGURE 13 Dual clamped patch test with $\nu = 0.49$. Comparison of the *Q1*, *Q1P0*, and *Q1P0F0* element formulations for fiber stifness values $\mu_f = \{10^2, 10^4, 10^6, 10^8\}$ [Colour figure can be viewed at wileyonlinelibrary.com]

setting by clamping the nodes against the motion in z-direction by setting $u_z = 0$ for all nodes recovering the plane-strain problem proposed in the work of Schröder.[55] The results of the first set of analysis for $\nu = 0.3$ are depicted in Figure 12. The left column depicts the horizontal displacement for the center of the left surface (see Figure 11). This example demonstrates a compressible material response for a variety of fiber stiffness values. As demonstrated in the third and fourth rows for $\mu_f = 10^6$ and $\mu_f = 10^8$, *Q1* and *Q1P0* formulations are divergent for increased mesh resolution. This is in line with the remarks of Ehlers and Eipper[52] for the volumetric and isochoric split of the free energy function in compressible range. The proposed *Q1P0F0* formulation is the most robust among all, showing no divergence throughout the whole set of simulations. The convergence of the middisplacement for increasing mesh density is also remarkable for the proposed

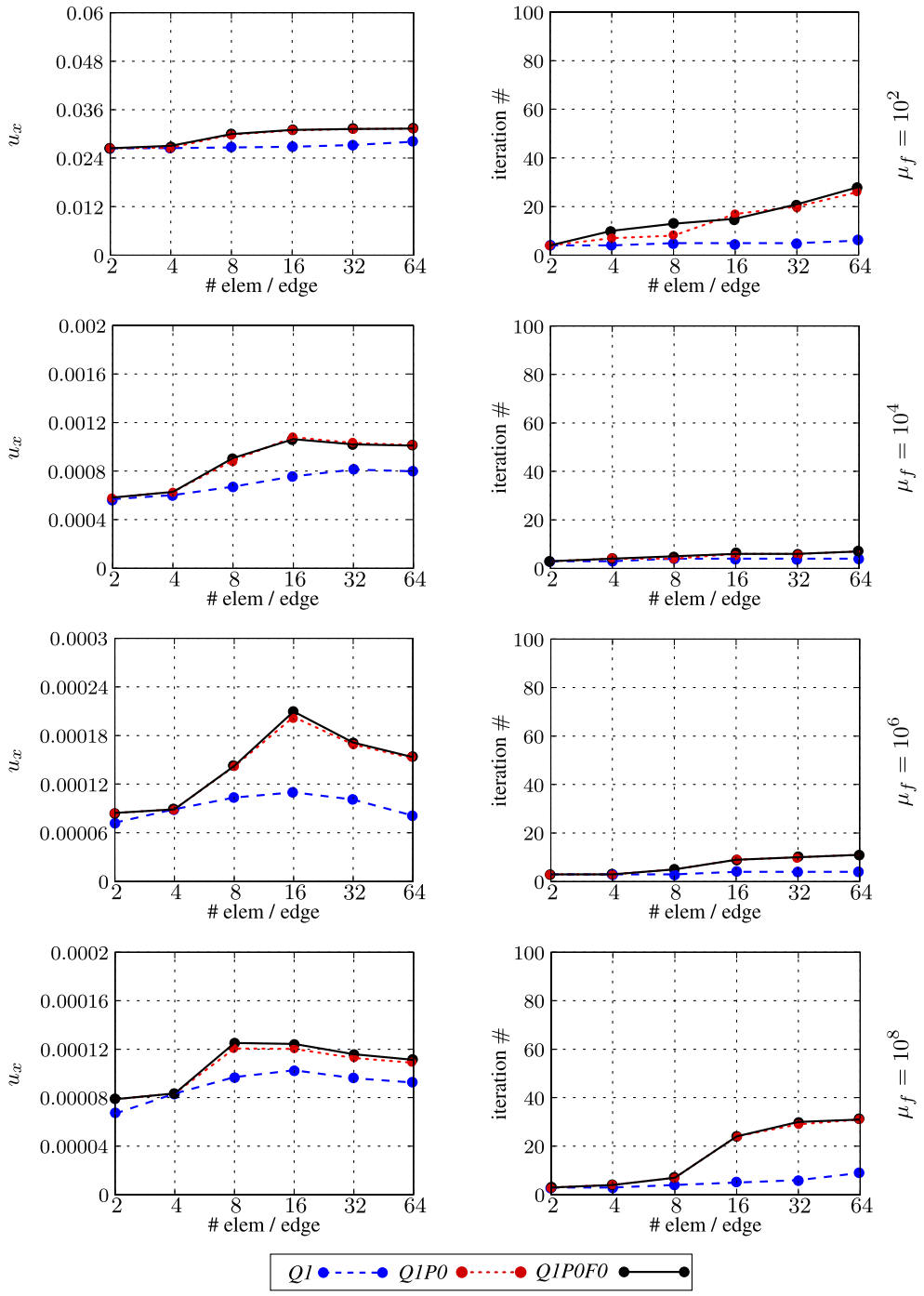

FIGURE 14 Dual clamped patch test with $\nu = 0.4999$. Comparison of the *Q1*, *Q1P0*, and *Q1P0F0* element formulations for fiber stiffness values $\mu_f = \{10^2, 10^4, 10^6, 10^8\}$ [Colour figure can be viewed at wileyonlinelibrary.com]

formulation. The simulations are repeated for $\nu = 0.49$ and $\nu = 0.4999$, and the results are depicted in Figure 13 and Figure 14, respectively. In both compressible and quasi-incompressible cases, for increasing μ_f, the predictions for the middisplacement u_x for *Q1* and *Q1P0* element formulations tend to be identical. However, for the case $\nu = 0.49$, both formulations are considerably stiff due to locking for coarse meshes. For number of elements/edge values of $\{8, 16, 32, 64\}$, the variation in the predictions from *Q1P0FO* are very small, where the predictions of *Q1* and *Q1P0* formulations converge to the predictions obtained from the *Q1P0FO* formulation. The proposed formulation is very robust and is the only formulation to converge through all set of parameters. The number of total iterations to the final solution is very low compared to the solutions proposed in the literature, especially in the quasi-incompressible and quasi-inextensible limit.[55] Finite element formulations based on lower order interpolations can yield a poor stress field and lead to stress oscillations. Fiber stress and hydrostatic stress plots obtained by three different formulations are compared for 32×32, 64×64, and 128×128 mesh densities in Figure 15 and Figure 16, respectively. For the postprocessing process, the standard L2-projection described in the theory manual of the academic purpose finite element program FEAP is used. The results do not show any stress oscillations, which were reported in the work of Schröder et al,[55] are very close to each other. The

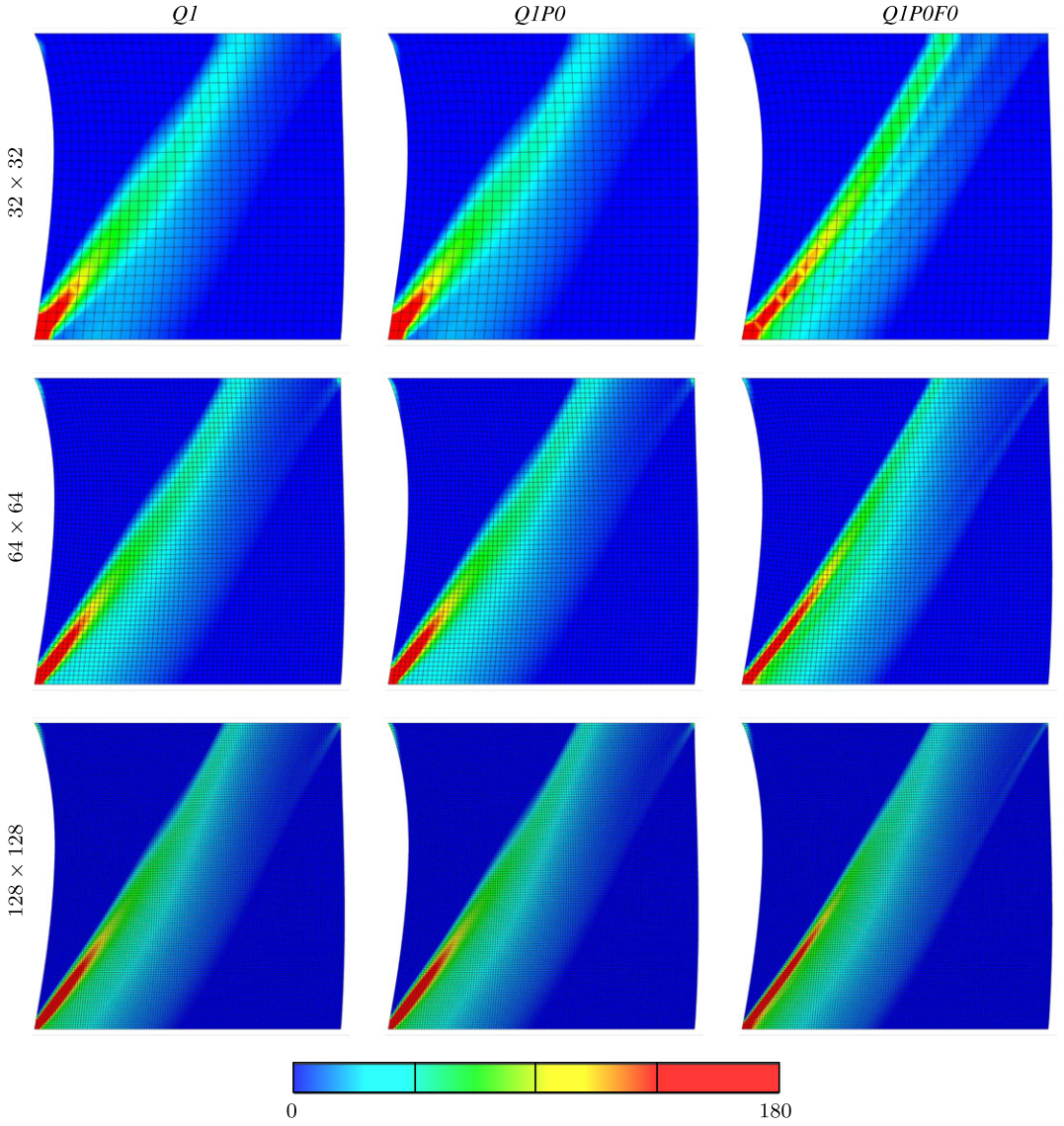

FIGURE 15 Dual clamped patch test with $\nu = 0.3$ and $\mu_f = 10^4$. Cauchy-type fiber stresses $\boldsymbol{\sigma}_f$ in the fiber orientation direction $\boldsymbol{f}$. The first, second, and third columns denote *Q1*, *Q1P0*, and *Q1P0F0* element formulations, for 32 elements/edge (first row), 64 elements/edge (second row), and 128 elements/edge (third row), respectively

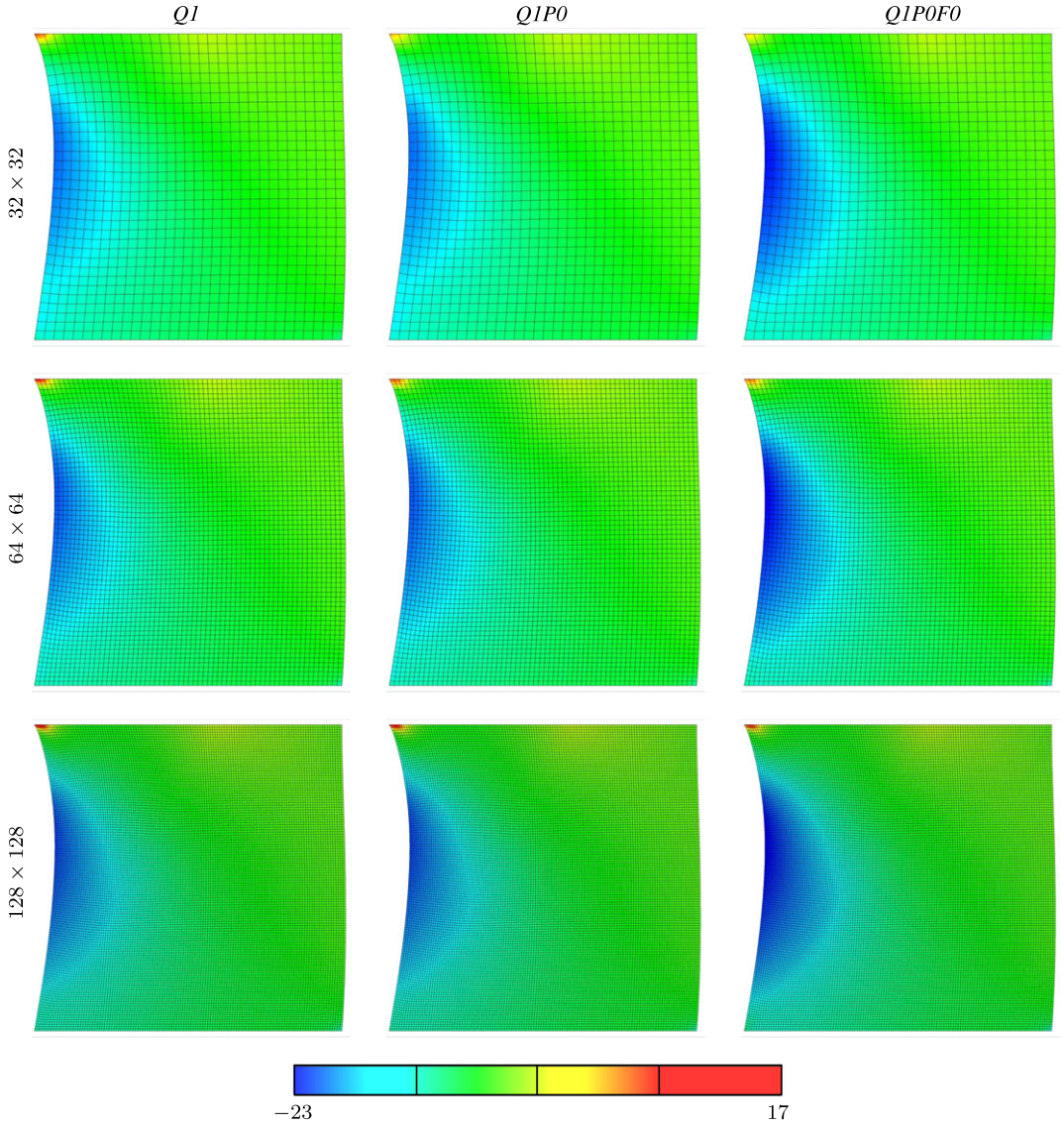

FIGURE 16 Dual clamped patch test with $\nu = 0.3$ and $\mu_f = 10^4$. Cauchy-type hydrostatic stresses p. The first, second, and third columns denote *Q1*, *Q1P0*, and *Q1P0F0* element formulations, for 32 elements/edge (first row), 64 elements/edge (second row), and 128 elements/edge (third row), respectively

minor deviation is due to the different choice of volumetric free energy function and use of invariants of the unimodular part of the right Cauchy-Green tensor in the current manuscript. However, it should be mentioned that the design of a new boundary value problem, which can act as a standard benchmark test for the inextensibility constraint, is an open issue to be exploited.

6 | REMARKS AND CONCLUSION

In this work, a five field Hu-Washizu–type variational principle for the quasi-incompressible and quasi-inextensible limit of transversely anisotropic materials at large strains is proposed. The material formulation is in the Eulerian setting. The advantage of the proposed formulation is the ease of implementation at element level where the additional degrees of freedoms are condensed out with numerical homogenization at element level. The formulation requires no matrix inversion operations, enabling fast and direct computation of element stiffness matrix. The proposed *Q1P0FO* formulation requires no additional kinematical assumptions, making it very suitable for the implementation of the so-called *standard reinforcing models* of transverse anisotropic solids. The extension of the *Q1P0* element formulation to *Q1P0FO* element

formulation requires very few additional algebraic operations and the implementation is straightforward. Besides, the compact structure, the proposed element, is very robust and exhibits good coarse mesh accuracy for the displacement field both at compressible and incompressible limit for transversely anisotropic solids. Future work will be devoted to the investigation of the performance of the proposed formulation for biological tissues.

ACKNOWLEDGEMENTS

The author gratefully acknowledges the financial support from Tübitak Bideb 2232 under grant number 114C073. The author also acknowledges the fruitful discussions with Burak Rodoplu, Yashar Badienia, and Pouya Zoghipour.

ORCID


H. Dal http://orcid.org/0000-0002-2973-3991

REFERENCES

1. Hughes TJR. Generalization of selective integration procedures to anisotropic and nonlinear media. *Int J Numer Methods Eng*. 1980;15:1413-1418.
2. Hughes TJR. *The Finite Element Method: Linear Static and Dynamic Finite Element Analysis*. Englewood Cliffs, NJ: Prentice Hall; 1987.
3. Zdunek A, Rachowicz W, Eriksson T. A novel computational formulation for nearly incompressible and nearly inextensible finite hyperelasticity. *Comput Methods Appl Mech Eng*. 2014;281:220-249.
4. Zdunek A, Rachowicz W, Eriksson T. A five-field finite element formulation for nearly inextensible and nearly incompressible finite hyperelasticity. *Comput Math Appl*. 2016;72:25-47.
5. Scott LR, Vogelius M. Norm estimates for a maximal right inverse of the divergence operator in spaces of piecewise polynomials. *Math Model Numer Anal*. 1985;19:111-143.
6. Simó J, Armero F, Taylor R. Improved versions of assumed enhanced strain tri-linear elements for 3D finite deformation problems. *Comput Methods Appl Mech Eng*. 1993;110:359-386.
7. Wriggers P. *Nonlinear Finite Element Methods*. Berlin, Germany: Springer-Verlag Berlin Heidelberg; 2008.
8. Pian THH, Chen DP. Alternative ways for formulation of hybrid stress elements. *Int J Numer Methods Eng*. 1982;18(11):1679-1684.
9. Pian THH. Derivation of element stiffness matrices by assumed stress distributions. *AIAA J*. 1964;2(7):1333-1336.
10. Pian THH, Sumihara K. Rational approach for assumed stress finite elements. *Int J Numer Methods Eng*. 1984;20(9):1685-1695.
11. Auricchio F, da Veiga LB, Lovadina C, Reali A. A stability study of some mixed finite elements for large deformation elasticity problems. *Comput Methods Appl Mech Eng*. 2005;194(9-11):1075-1092.
12. Malkus DS, Hughes TJR. Mixed finite element methods – reduced and selective integration techniques: a unification of concepts. *Comput Methods Appl Mech Eng*. 1978;15(1):63-81.
13. Zienkiewicz OC, Taylor RL, Too JM. Reduced integration technique in general analysis of plates and shells. *Int J Numer Methods Eng*. 1971;3(2):275-290.
14. Belytschko T, Ong JSJ, Liu WK, Kennedy JM. Hourglass control in linear and nonlinear problems. *Comput Methods Appl Mech Eng*. 1984;43(3):251-276.
15. Reese S, Küssner M, Reddy BD. A new stabilization technique for finite elements in non-linear elasticity. *Int J Numer Methods Eng*. 1999;44(11):1617-1652.
16. Belytschko T, Bindeman LP. Assumed strain stabilization of the eight node hexahedral element. *Comput Methods Appl Mech Eng*. 1993;105(2):225-260.
17. Simó JC, Armero F. Geometrically non-linear enhanced strain mixed methods and the method of incompatible modes. *Int J Numer Methods Eng*. 1992;33(7):1413-1449.
18. Simó JC, Hughes TJR. On the variational foundations of assumed strain methods. *J Appl Mech*. 1986;53:51-54.
19. Simó JC, Rifai MS. A class of mixed assumed strain methods and the method of incompatible modes. *Int J Numer Methods Eng*. 1990;29(8):1595-1638.
20. de Souza Neto E, Perić D, Dutko M, Owen D. Design of simple low order finite elements for large strain analysis of nearly incompressible solids. *Int J Solids Struct*. 1996;33(20-22):3277-3296.
21. Hu HC. On some variational principles in the theory of elasticity and the theory of plasticity. *Acta Phys Sin*. 1954;10(3):259-290.
22. Washizu K. On the variational principles of elasticity and plasticity. Cambridge, UK: M.I.T. Aeroelastic and Structures Research Laboratory; March 1955.
23. Miehe C, Aldakheel F, Mauthe S. Mixed variational principles and robust finite element implementations of gradient plasticity at small strains. *Int J Numer Methods Eng*. 2013;94(11):1037-1074.
24. Miehe C, Teichtmeister S, Aldakheel F. Phase-field modelling of ductile fracture: a variational gradient-extended plasticity-damage theory and its micromorphic regularization. *Philos Trans Royal Soc Lond A Math Phys Eng Sci*. 2016;374(2066).
25. Miehe C, Welschinger F, Aldakheel F. Variational gradient plasticity at finite strains. Part II: local–global updates and mixed finite elements for additive plasticity in the logarithmic strain space. *Comput Methods Appl Mech Eng*. 2014;268:704-734.

26. Glaser S, Armero F. On the formulation of enhanced strain finite elements in finite deformations. *Eng Comput*. 1997;14(7):759-791.
27. Korelc J, Wriggers P. Consistent gradient formulation for a stable enhanced strain method for large deformations. *Eng Comput*. 1996;13:103-123.
28. Reese S, Wriggers P. A stabilization technique to avoid hourglassing in finite elasticity. *Int J Numer Methods Eng*. 2000;48(1):79-109.
29. Wriggers P, Reese S. A note on enhanced strain methods for large deformations. *Comput Methods Appl Mech Eng*. 1996;135:201-209.
30. Nagtegaal JC, Parks DM, Rice JR. On numerically accurate finite element solutions in the fully plastic range. *Comput Methods Appl Mech Eng*. 1974;4:153-177.
31. Brezzi F, Fortin M. *Mixed and Hybrid Finite Element Methods*. New York, NY: Springer-Verlag; 1991.
32. Simó JC, Taylor RL, Pister KS. Variational and projection methods for the volume constraint in finite deformation elasto-plasticity. *Comput Methods Appl Mech Eng*. 1985;51(1-3):177-208.
33. Simó JC, Taylor RL. Quasi-incompressible finite elasticity in principal stretches. Continuum basis and numerical algorithms. *Comput Methods Appl Mech Eng*. 1991;85:273-310.
34. Miehe C. Aspects of the formulation and finite element implementation of large strain isotropic elasticity. *Int J Numer Methods Eng*. 1994;37(12):1981-2004.
35. Dal H, Kaliske M. Bergström–Boyce model for nonlinear finite rubber viscoelasticity: theoretical aspects and algorithmic treatment for the FE method. *Comput Mech*. 2009;44(6):809-823.
36. Weiss JA, Maker BN, Govindjee S. Finite element implementation of incompressible, transversely isotropic hyperelasticity. *Comput Methods Appl Mech Eng*. 1996;135(1-2):107-128.
37. Babuška I. The finite element method with Lagrangian multipliers. *Numer Math*. 1973;20(3):179-192.
38. Brezzi F. On the existence, uniqueness and approximation of saddle-point problems arising from Lagrangian multipliers. *Revue française d'autom informatique recherche opér Anal numér*. 1974;8:129-151.
39. Ladyžhenskaya O. *The Mathematical Theory of Viscous Incompressible Flow*. Vol. 76. New York, NY: Gordon and Breach; 1969.
40. Bathe K-J. The inf–sup condition and its evaluation for mixed finite element methods. *Comput Struct*. 2001;79:243-252.
41. Spencer A. *Deformations of Fibre-Reinforced Materials*. Oxford, UK: Oxford University Press; 1972.
42. Boehler J-P. A simple derivation of representations for non-polynomial constitutive equations in some cases of anisotropy. *ZAMM - Zeitschrift Angewandte Math Mech*. 1979;59(4):157-167.
43. Betten J. Formulation of anisotropic constitutive equations. In: *Applications of Tensor Functions in Solid Mechanics*. Vienna, Austria: Springer, Vienna; 1987;228-250. *International Centre for Mechanical Sciences*; vol. 292.
44. Schröder J, Neff P. Invariant formulation of hyperelastic transverse isotropy based on polyconvex free energy functions. *Int J Solids Struct*. 2003;40(2):401-445.
45. Qiu G, Pence T. Remarks on the behavior of simple directionally reinforced incompressible nonlinearly elastic solids. *J Elast*. 1997;49(1):1-30.
46. Holzapfel GA, Gasser TC, Ogden RW. A new constitutive framework for arterial wall mechanics and a comparative study of material models. *J Elast Phys Sci Solids*. 2000;61(1-3):1-48.
47. Qiu GY, Pence TJ. Loss of ellipticity in plane deformation of a simple directionally reinforced incompressible nonlinearly elastic solid. *J Elast*. 1997;49(1):31-63.
48. Merodio J, Ogden RW. Material instabilities in fiber-reinforced nonlinearly elastic solids under plane deformation. 2002;54(5-6):525-552.
49. Merodio J, Ogden RW. Instabilities and loss of ellipticity in fiber-reinforced compressible non-linearly elastic solids under plane deformation. *Int J Solids Struct*. 2003;40(18):4707-4727.
50. Adkins JE, Rivlin RS. Large elastic deformations of isotropic materials X. Reinforcement by inextensible cords. *Philos Trans Royal Soc Lond Ser Math Phys Sci*. 1955;248(944):201-223.
51. Flory PJ. Thermodynamic relations for highly elastic materials. *Trans Faraday Soc*. 1961;57:829-838.
52. Ehlers W, Eipper G. The simple tension problem at large volumetric strains computed from finite hyperelastic material laws. *Acta Mech*. 1998;130(1-2):17-27.
53. Sansour C. On the physical assumptions underlying the volumetric-isochoric split and the case of anisotropy. *Eur J Mech A/Solids*. 2008;27(1):28-39.
54. Helfenstein J, Jabareen M, Mazza E, Govindjee S. On non-physical response in models for fiber-reinforced hyperelastic materials. *Int J Solids Struct*. 2010;47:2056-2061.
55. Schröder J, Viebahn N, Balzani D, Wriggers P. A novel mixed finite element for finite anisotropic elasticity; the SKA-element simplified kinematics for anisotropy. *Comput Methods Appl Mech Eng*. 2016;310:475-494.
56. Wriggers P, Schröder J, Auricchio F. Finite element formulations for large strain anisotropic material with inextensible fibers. *Adv Model Simul Eng Sci*. 2016;3:1-18.
57. Demarco D, Dvorkin EN. An Eulerian finite element formulation for modelling stationary finite strain elastic deformation processes. *Int J Numer Methods Eng*. 2005;62(8):1038-1063.
58. Oñate E, Carbonell JM. Updated Lagrangian mixed finite element formulation for quasi and fully incompressible fluids. *Comput Mech*. 2014;54(6):1583-1596.
59. Marsden JE, Hughes TJR. *Mathematical Foundations of Elasticity*. Englewood Cliffs, NJ: Prentice-Hall; 1983.

60. Ogden RW. Large deformation isotropic elasticity: on the correlation of theory and experiment for compressible rubberlike solids. *Proc R Soc Lond A Math Phys Sci*. 1972;328(1575):567-583.

61. Yeoh OH. Some forms of the strain energy function for rubber. *Rubber Chem Technol*. 1993;66(5):754-771.

62. Hartmann S, Neff P. Polyconvexity of generalized polynomial-type hyperelastic strain energy functions for near-incompressibility. *Int J Solids Struct*. 2003;40(11):2767-2791.

How to cite this article: Dal H. A quasi-incompressible and quasi-inextensible element formulation for transversely isotropic materials. *Int J Numer Methods Eng*. 2019;117:118–140. https://doi.org/10.1002/nme.5950